Energy Geoscience 2 (2021) 10–31

Contents lists available at ScienceDirect

Energy Geoscience

journal homepage: www.keaipublishing.com/en/journals/energy-geoscience

Diagenesis and its controls on reservoir quality of the Tambar oil field, Norwegian North Sea

Mohammed Bukar [a, *], Richard H. Worden [b], Shettima Bukar [b], Philip Shell [c]

[a] Department of Earth and Ocean Sciences, University of Liverpool, Liverpool, L69 3GP, UK
[b] Department of Geology, University of Maiduguri, Nigeria
[c] Saudi Aramco, Al-Dhahran, Eastern Region, Saudi Arabia

ARTICLE INFO

Article history:
Received 12 April 2020
Received in revised form
24 June 2020
Accepted 7 July 2020

Keywords:
Diagenesis
Oil-inhibition
Microquartz-inhibition
Anomalous porosity
Permeability

ABSTRACT

A study of the diagenetic evolution of the Late Jurassic sandstones of the shallow marine facies in the Tambar oil field, Norwegian North Sea was carried out to understand its controls on reservoir quality. Core samples and a set of wireline logs obtained from three wells were used to carry out petrographic studies including light optics and scanning electron microscopy, well log analysis, fluid inclusions, X-ray diffraction (XRD) for whole rock samples, clay mineral extracts and stable isotopes. The Tambar reservoir sandstones range mainly from siltstone to fine-grained sandstones, exclusively arkoses cemented mainly by microcrystalline quartz, euhedral quartz overgrowth, dolomite cement, illite and chlorite. Early diagenetic/eodigenetic minerals include pyrite, calcite, and microcrystalline quartz and late diagenetic/mesodiagenetic minerals include quartz overgrowth, dolomite, illite and chlorite. The $\delta^{18}O$ values of dolomite cement in the Tambar sandstone reservoir range from −11.77‰ to −3.57‰ PDB, while the $\delta^{13}C$ values of the dolomite cement are from −5.07‰ to −1.12‰ PDB. Homogenization temperature for fluid inclusions trapped in authigenic quartz fall between 130 °C and 169 °C. The reservoir quality is controlled mainly by early formed grain-coating microcrystalline quartz that precipitated from the dissolution of sponge spicules which significantly inhibits quartz overgrowth precipitation. Oil emplacement do not show significant control on reservoir quality because considerable quartz cementation has taken place before the onset of major oil charge. Only the coarse-grained sands show a correlation between quartz cement volume and water saturation. However, the interpreted temperature for dolomite cementation is significantly higher for water leg-suggested effect of oil emplacement on the late dolomite. Understanding these controls on the reservoir quality will enhance the exploration strategy for the Tambar oil field.

1. Introduction

The Tambar oil field is described as part of Ula trend because of its proximity to the main Ula oil field (16 km to the north) (O'Connor et al., 2011). Considerable interest has been drawn over the last few decades to the reservoir potential of the Upper Jurassic sandstones of the Central Graben area of the North Sea (Home, 1987; Karlsen et al., 1993; Karlsen and Skeie, 2006; Knipe et al., 1991; Nedkvitne et al., 1993; Oxtoby et al., 1995; Stewart, 1993). Most studies have been performed at the regional level or on the Ula field; few studies have been carried out specifically on the reservoir properties and factors controlling the reservoir quality of the Tambar oil field. The present study aims to fill the gap and gives account of how sandstone composition and diagenetic activity have affected reservoir quality of the Tambar oil field.

Sandstones buried to a depth of greater than 2500 m and exposed to high lithostatic pressure tend to have loose porosity mainly through a combination of compaction and cementation (Ehrenberg, 1990). Compaction includes mechanical compaction

* Corresponding author. Geology Department, University of Maiduguri Nigeria, , Nigeria.
E-mail address: bukarmohammed2@unimaid.edu.ng (M. Bukar).

Production and Hosting by Elsevier on behalf of KeAi

https://doi.org/10.1016/j.engeos.2020.07.002

(rearrangement of grains, grain bending, grain fracturing) and chemical compaction (pressure solution at grain contacts or along stylolite seams). Cementation occurs when sediment-fluid systems are out of geochemical and textural equilibrium; they tend to interact progressively as the ambient environment evolves in terms of temperature, pressure and fluid chemistry during burial. The result is the precipitation of new mineral cements that is in, or approaching, equilibrium with new burial environment. The new cements tend to result in the blocking of pore throats to reduce porosity. The most common cements are quartz (as overgrowth), pore-filling dolomite, and pore-throat blocking clays such as illite. However, porosity can be preserved in deeply buried sandstones by: (1) early diagenetic microquartz coatings (Aase et al., 1996; Jahren and Ramm, 2000; Lima and De Ros, 2002), (2) the presence of early diagenetic chlorite coatings (Ajdukiewicz et al., 2010; Bloch et al., 2002; Dixon et al., 1989), (3) overpressure (Osborne and Swarbrick, 1999; Ramm and Bjorlykke, 1994), and (4) early oil emplacement (Gluyas et al., 1993; Marchand et al., 2001; Wilkinson and Haszeldine, 2011). Microquartz and chlorite coatings preserve porosity by inhibiting quartz cementation, whereas overpressure limits compaction and potentially inhibits pressure solution (Sheldon et al., 2003). Early emplacement of oil into a reservoir potentially limits diagenetic activity thereby stopping precipitation of cements (Kraishan et al., 2000; Worden et al., 1998, 2018).

Reservoir quality is controlled by interdependent sedimentary and diagenetic factors, including the origin of a sediment (provenance), depositional environment, weathering and climate conditions both in the hinterland and at the site of deposition, compaction, recrystallization and dissolution, authigenic mineral growth, petroleum charge, burial depth, extent and rate of heating, fluid pressure and effective stress, and structural deformation (Morad et al., 2012).

Porosity controls oil and gas reserve volumes and permeability controls the flow rate of the produced oil to surface. Thus understanding what controls porosity and permeability is crucial for predicting reservoir quality and so determining the economic viability and development strategy of a given oil or gas field. Although Tambar sits relatively close to Ula, it has been reported to be different and less good in terms of reservoir quality for some obscure reasons. Therefore, a diagenetic analysis has here been undertaken to understand the diagenesis and its effect on the reservoir quality of the Tambar oil field. Specific questions to be addressed are as follows:

- What are the most significant diagenetic mineral cements in the Tambar oil field?
- What is the sequence of diagenetic mineral growth?
- What are the sources and processes that have resulted in these minerals?
- What controls porosity and permeability in the Tambar oil field?
- Have any processes led to the inhibition of quartz cement growth and preservation of porosity?

2. Geological background

Tambar (Norwegian: *Tambarfeltet*) is an offshore oil field located in the southern Norwegian section of North Sea, along with Ula and Gyda fields making up the UGT area (Fig. 1). The North Sea Basin began as the Appalachian - Caledonian Geosyncline in the Cambrian - Devonian. The geosyncline was once part of a large mountain belt which extended from Greenland and Norway over to the southeast of North America. This orogeny resulted in the combination of western Europe and North America. Later, this area subsided and eroded into a horst and graben structure which has resulted in the red sandstones that make up many of the reservoirs in the basin. Then, rifting occurred in this region creating two intercratonic basins of different formation age. The northern basin formed during the Late Devonian and the southern basin during the Carboniferous (Allen and Mange-Rajetzky, 1992). The Tambar oil field area is a major geological structure that was tectonically active from the Middle Jurassic through to the Late Cretaceous probably due to the collapse of the Zachstein salt. It forms part of the Central Graben where shallow marine Jurassic sands were deposited in salt-dissolution features separated by inverted Triassic pods (O'Connor et al., 2011). The Central Graben is characterized by several narrow, discontinuous structural highs and lows (Skjerven et al., 1983), with a very complicated tectonic history.

The formations in the Tambar oil field consists of the Vestland Group, Tyne Group, Cromer knoll Group, Shetland Group, Rogaland Group and the Hordland Group (Fig. 2). The Vestland Group consists of the Ula Formation which was deposited on the Triassic Skaggarak Formation. The Ula Formation consists of very fine-to medium-grained, moderately to well sorted sandstone and mudstone toward the lower part. The Tyne Group is made up of the Farsund and Mandal Formations. The Farsund Formation is composed of a lower Gyda sandstone member and an upper mudstone member. In some company reports (Completion Logs etc.), the Gyda sandstone member is considered to be part of the Ula Formation. The Mandal Formation is the local stratigraphic name for the Kimmeridge Clay Formation, which is more typically used by authors in the Central Graben area (Hamar et al., 1983). Mudstones and argillaceous limestones of the Lower Cretaceous Cromer Knoll Group overlie the Upper Jurassic of the Mandal Formation. The Cromer Knoll is made up of Asgard, Tuxen, Sola and Rødby Formations which are dominantly mudstones. It is overlain by the Late Cretaceous to Early Tertiary carbonate-dominated Shetland Group (also known as the Chalk) comprising of the Ekofisk, Tor and Hod Formations. The Eocene Rogaland Group comprising the Vale, Lower Lista, Vidar, Upper Lista, Sele and Balder Formations overlies the Shetland Group. The undifferentiated Hordland Group is the topmost sediments in the Tambar oil field.

The pay horizons in the Tambar oil field are confined to the Upper Jurassic Ula Formation and the Gyda sandstone member of the Farsund Formation (Fig. 2) (Bergan et al., 1989; Karlsen et al., 1993; Partington et al., 1993; Underhill, 1998). From the neighbouring Ula field, this unit has been described as a shallow marine sandstone of up to 200 m thick that prograded across outer-shelf mudstones, following a sea level fall in the Kimmeridgian (Harris, 2006). The Ula Formation sandstones are typically fine-grained, well sorted and highly bioturbated with beds rich in lithic shale fragments. The Ula Formation unconformably overlies the partly-eroded Middle Jurassic and Triassic fluvial Skagerrak Formation (Fig. 2). This unit is in turn overlain by the Late Jurassic mudstones, which include the Upper Jurassic source rocks (Wilhelms and Larter, 1994). The shale member of the Farsund Formation and especially the overlying Mandal Formation are likely to be the local source rocks, as is the case of the adjacent Ula field and oil fields in the neighbouring Danish sector (Petersen et al., 1AD).

The reservoir temperature recorded from bottom hole (at a depth of 4272 m) measurements of Well 1/3-3 is 179 °C. The Tambar oil field seems to have had a relatively simple burial and thermal history with the Ula Formation being progressively buried, with no notable periods of uplift or cooling. The Ula Formation reached 90 °C at about 60Ma, 130 °C at about 25Ma and 160 °C at about 2Ma (Fig. 3).

3. Materials and methods

Wireline and conventional core analysis data from the Tambar

oil field were made available by BP Norway. Core plugs were taken at 30 cm-spacings with porosity and permeability measured using industry-standard methods. The downhole wireline logs available are: calliper, bulk density, neutron porosity, sonic transit time, bulk gamma, shallow resistivity and deep resistivity. Wireline data were reported every 10 cm from the Ula Formation from each of the three wells sampled in the Tambar oil field. Porosity was calculated for each of the logs using the density log (Serra, 1984; Collet, 1998; Collet and Ladd, 2000; Rider and Kennedy, 2011; Worden et al., 2018, 2020) and the following relationship is thereby obtained:

$$\text{Fractional porosity} = (\rho_{mbd} - \rho_{amd})/(\rho_{fd} - \rho_{amd}) \quad \text{(eq. 1)}$$

Where:

ρ_{mbd} = measured bulk density (from wireline logs)
ρ_{amd} = average mineral density
ρ_{fd} = fluid density

The average mineral density employed is 2.66 g/cm^3. The average fluid density is taken as 1.00 g/cm^3 since the fluid in the zone next to the well bore will be aqueous due to the water-based drilling fluids replacing the initial pore fluid (predominantly oil in the oil leg). The results of the wireline calculation of porosity are compared to the core analysis porosity to check credibility (Fig. 4). The porosity and permeability data obtained by conventional core analysis are provided by the operating oil company (BP) from the cored sections of the Ula Formation (Fig. 5).

Water saturation is calculated from the wireline data for each depth using the Archie equation:

$$S_w = [(a/Ø^m)/(R_w/R_t)]^{(1/n)} \quad \text{(eq. 2)}$$

Where:

S_w = fractional water saturation
n = saturation exponent
a = tortuosity constant
R_w = formation water resistivity (determined at reservoir temperature)
R_t = formation resistivity (obtained from deep resistivity log to reduce any effect of drilling mud).
Ø = density log-derived fractional porosity (see eq. (1))
m = cementation exponent

Values of n, a, and m are fixed at 2.5, 0.82 and 2.0 respectively as used by the field development geoscientists. Only deep induction resistivity measurements were used in the formula, as these are the only resistivity measurements that give true formation resistivity, unaffected by invasion of drilling fluids into the formation(Asquith and Gibson, 1982). Water resistivity was 0.025 Ω/m (Oxtoby, 1994).

Seventy-seven samples of conventional core plugs from the

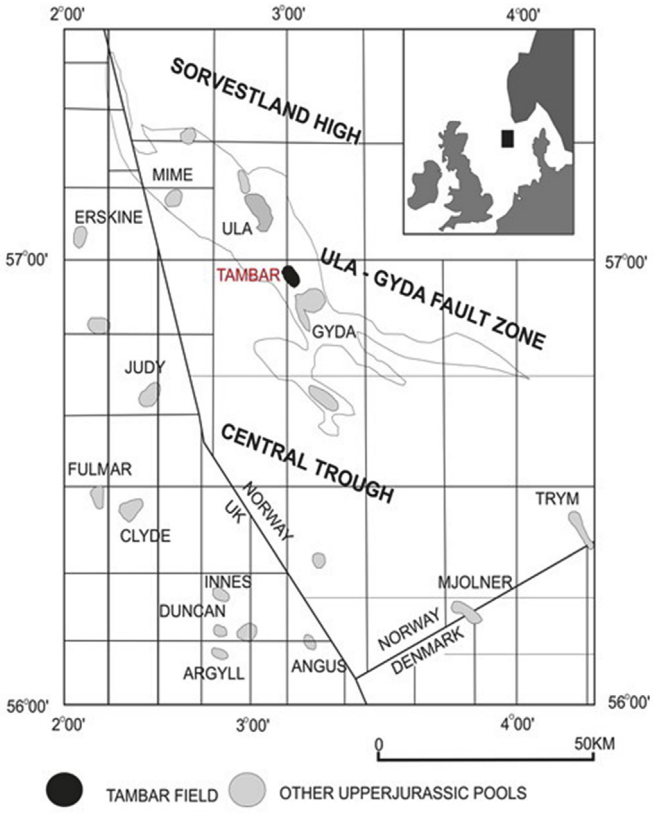

Fig. 1. Location map of the Tambar oil field in the Central Graben, North Sea (modified from Bjørnseth and Gluyas, 1995).

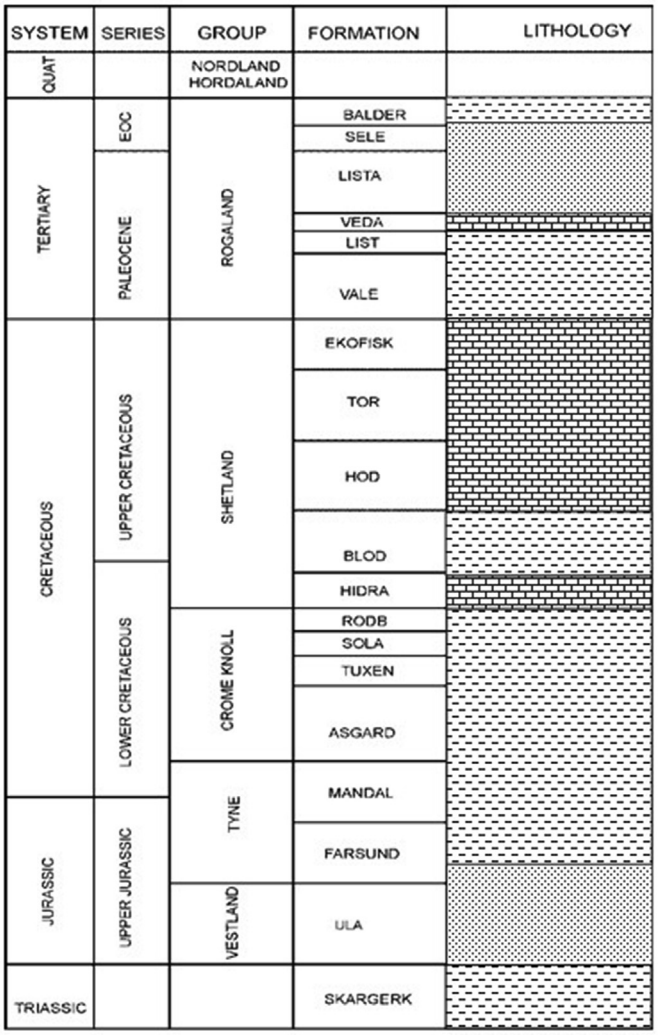

Fig. 2. Simplified stratigraphy of the Tambar oil field produced from Well 1/3-3 (data used from BP well report).

three wells were obtained from the BP core store at Reslab laboratories in Stavanger, Norway. The core sample suit covers the range of present subsurface at a measured depth varying from 4130 m to 4373 m, and spans the thickness of the whole reservoir. Individual sandstones were studied using a combination of techniques, including petrography, scanning electron microscopy (SEM), cathodoluminescence microscopy (CL), X-ray diffraction (XRD) and fluid inclusion micro-thermometry.

Polished thin sections were made from the core samples. The polished sections were impregnated with blue resin in order to highlight porosity. Sandstone modal composition was obtained by detail point counts (400 counts per section) of all thin sections. Grain sizes and grain coating were measured using Meiji 9000 microscope fitted with an Infinity 1.5 camera. Images were snapped and long axes of 100 grains were measured using Infinity Analyser software. Fifty grains per section was measured for the percentage of grain-coating microcrystalline quartz coverage using visual estimates. Only potential sites for quartz cementation (i.e., facing pores, not coated with dead-oil or clay matrix) that were coated with microcrystalline quartz were measured and expressed as a percentage of all potential sites for quartz cementation.

SEM examinations were made using a Philips XL 30 SEM with tungsten filament with an accelerating voltage of 20 kV, and 8 nA beam current for both SE and BSEM. The SEM study was carried out on polished sections and freshly fractured, stub-mounted samples coated with carbon and gold respectively. Energy dispersive X-ray analysis (EDAX) provided qualitative compositional analysis of clay minerals, carbonate cements and feldspars. Some of the sandstone samples were soaked in acetone to remove the oil stains which caused problems for the vacuum system in the gold coater. The CL images were collected at 10 Kv and spot size 7. They were collected by integrating the signal of 16 frames using a slow scanning raster which took about 8 min to collect. Samples for XRD were cut from the core samples.

PANalytical X'pert pro MPD X-ray diffractometer was used for the XRD analysis. Samples were crushed using micromill and distilled water for 10 min. They were then dried overnight in a low temperature oven and powdered using agate pestle and mortar. A copper X-ray source operating at 40 kV and 40 mA was used. Powder samples were loaded into cavity holders and rotated continuously during the scan, completing one rotation every 2 s. Programmable anti-scatter slits and a fixed mask were maintained in an irradiated sample area of 10 × 15 mm, with an additional 2° incident beam anti-scatter slit producing a flat background for raw data down to a 2 theta angle of 3°. The X'Celerator detector was set to scan in a continuous mode with full length active pulse-height discrimination levels set to 45%–80%. Operation of X-ray Diffractometer and Software was set using "HighScore Plus ®" analysis software and automated Rietveld refinement methods with reference patterns from the International Centre for Diffraction Data, Powder Diffraction File-2 Release 2008.

Fluid inclusion microthermometric studies were carried out on selected samples. Doubly polished fluid inclusion wafers were prepared from the core samples at the University of Birmingham. An Olympus BX-60 petrographic microscope was used for thermometry and was equipped with a Linkam THMSG 600 heating and cooling stage which enabled the measurement of the phase transition temperature from -180^0 to 600 °C with an accuracy of ±0.1 to ±1.0. Observations were made with different magnifications (objectives of 10x, 20x, 50x and 100x). Inclusions were photographed with Digital Camera Olympus DP71 for the purpose of fast mapping of inclusion locations. Homogenization temperature measurements were made on each inclusion in each small piece of fluid inclusion wafer and then freezing point depression measurements were made on each inclusion to prevent modification of the homogenization temperature (Worden et al., 1995). All fluid inclusion samples were also studied using UV-luminescence by Olympus BX-60 microscope. A super high pressure mercury lamp was used to provide the light, the purpose of which was to check for the possible presence of oil inclusions.

For stable-isotope analysis of diagenetic carbonates, the bulk compositions of dolomite cemented samples were used. The powders were prepared and XRD was carried out in order to preselect samples with only dolomite cements (no calcite). The dolomite samples were corrected for the effects of kinetic oxygen isotope fractionation associated with the production of CO_2 by the reaction of dolomite with phosphoric acid at 50 °C using a fractionation factor of 1.01066 (Rosenbaum and Sheppard, 1986). Only a few of the selected dolomite samples were able to liberate normal δ notation relative to PDB (Craig, 1957), and oxygen isotope was converted to SMOW for comparison using equation (Friedman and O'Neil, 1977).

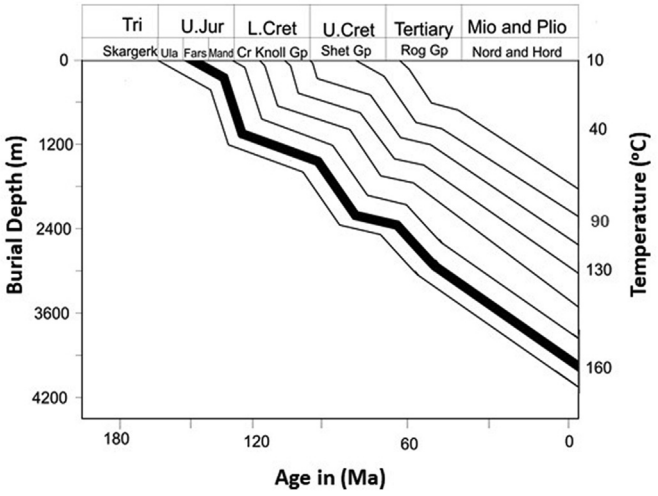

Fig. 3. Burial history curve of the Tambar oil field showing related tectonic events, temperatures, reservoir rocks in grey (data used from BP well report).

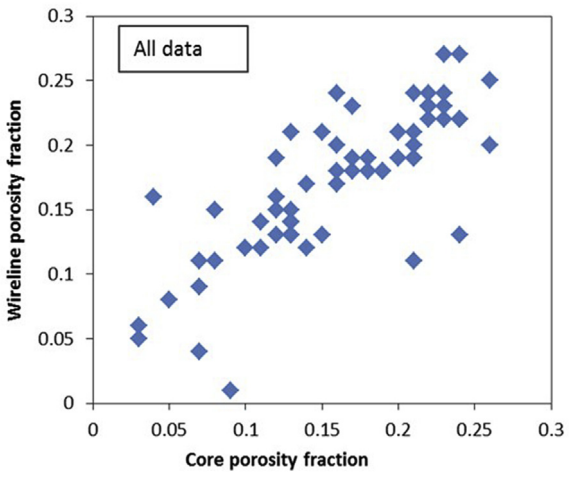

Fig. 4. Calibration of wireline porosity against core analysis porosity for the Ula sandstones of the Tambar oil field (wireline porosity derived from the density log data).

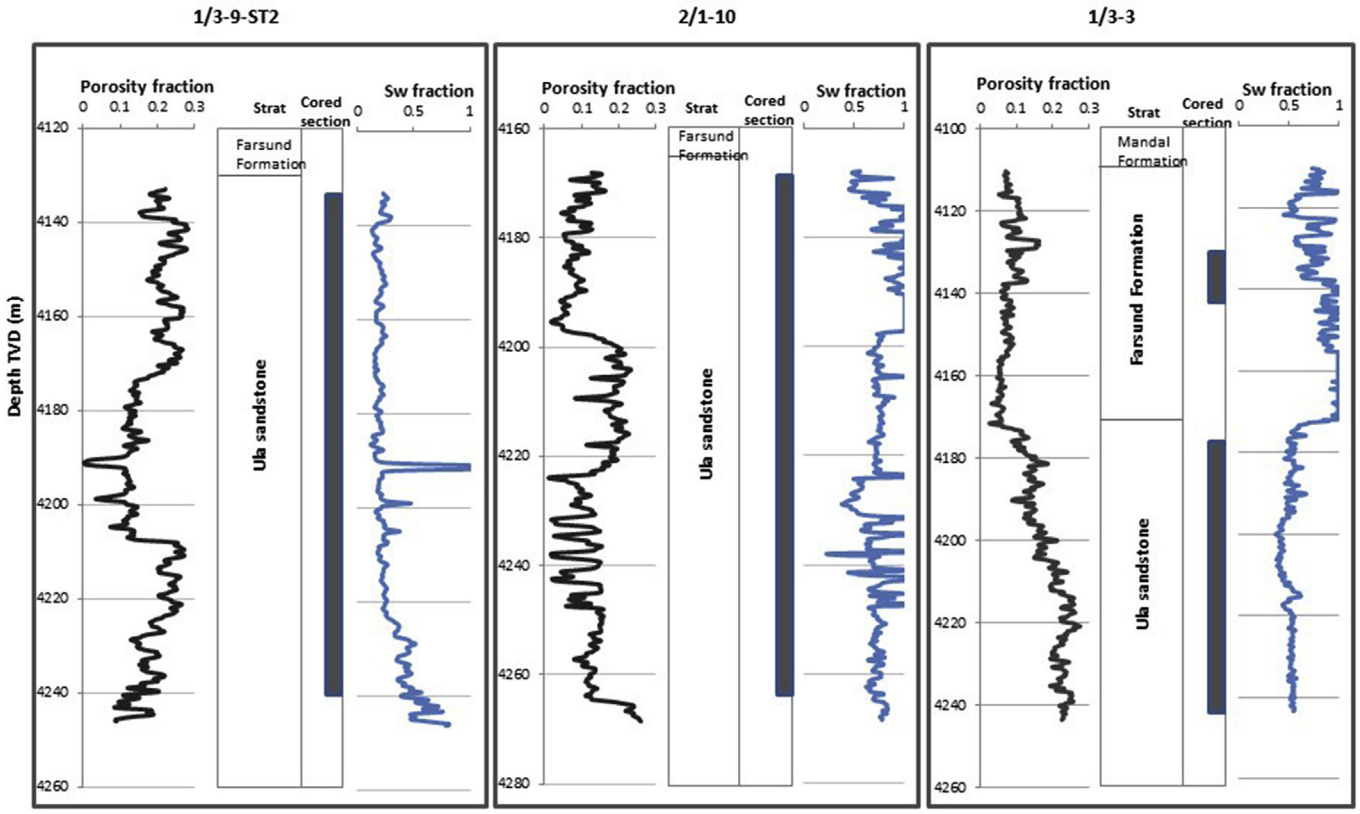

Fig. 5. Interpreted porosity from the density log (Fig. 4) and interpreted water saturations calculated from the resistivity log and using the Archie equation for the three wells in Tambar used in this study.

4. Results

4.1. Wireline analysis

For the studied sections in the three wells, density-derived porosity values range from as high as 27%–28% to as low as 0% (Fig. 5). The interpreted water saturation varies from 100% to a minimum of about 10%.

In Well 1/3-9-ST2, the Ula Formation has a water saturation approaching 100% at about 4245mTVD above which it progressively decreases to 10%–20% right up to the top of the cored section at about 4135mTVD. There are variations of porosity with what looks like two thick sequences of increasing reservoir quality upstratigraphy.

Two spikes of 100% water saturation and very low porosity represent two carbonate cemented intervals. This well is predominantly in the oil leg of Tambar field.

In Well 2/1-10, the Ula Formation has a relatively high water saturation throughout much of the section and is conventionally considered to represent the water leg of the oil field. The porosity is fairly low throughout this well except for an interval between about 4220 and 4240 m TVD where the porosity approaches 20%. In Well 1/3-3, the Ula Formation has a water saturation of as low as about 40% up to about 4180mTVD above which it suddenly increases to 100%. Whereas the depth matches a decrease in porosity from 25% down to a few percent, representing the stratigraphic top of the reservoir (the shale-rich Farsund Formation) (Fig. 5). The porous reservoir rocks largely sit within the oil leg in this well but have notably low maximum oil saturations.

4.2. Detrital grains, minerals and textures

Classification of the detrital mineralogy of the Tambar reservoir sandstones was performed using ternary plots (Folk, 1968); they fall into arkose class (Fig. 6) since they are relatively rich in detrital feldspars but contain few lithic fragments. Point count results show that the most abundant detrital grain is monocrystalline quartz (accounting for 34% on average of the rock volume, about 60% of the detrital grain mineralogy (Figs. 6 and 7; Table 1), with minor polycrystalline quartz (accounting for 3% on average). Feldspars represent about 25% of the rock volume and are volumetrically the second most important group of minerals. Tambar reservoir clastic rocks range from very fine-to fine-grained sandstones, and locally are silty. Grain sizes tend to be little above 250 μm and have been divided into three classes (<125 μm, 125-177 μm and >177 μm). They are moderately to well sorted (Fig. 7). The grains are dominantly sub-angular to sub-rounded.

The detrital feldspars include K-feldspar (12% on average) and plagioclase (12% on average) (Table 1). The majority of the K-feldspar and some plagioclase grains have undergone dissolution (Fig. 8). Total grain dissolution occurs locally leaving traces of replacive illite (Fig. 8C), which has resulted in a secondary porosity of up to 7% in some samples. Rock fragments are generally rare (<3%) in all samples (Table 1). Detrital clay occurs in patches and thin lenses (Fig. 9A). There are no apparent systematic compositional variations in mineralogy between wells or at different depths within wells.

Mica, mainly muscovite, occurs in variable amounts (1%–3% in volume). The muscovite grains are flat or platy but deformed when found between two detrital grains. Micas have apparently caused

dissolution of quartz grains since they are flattened at quartz-mica grain contact (Fig. 7C).

Other detrital minerals that occur in small amounts (<1% in volume) include glauconite, chalcedony, chert or bioclast, and heavy minerals (zircon, epidote, tourmaline, rutile, apatite, garnet and Fe-Ti oxides). The glaucony grains are olive green in colour, and typically under strong deformation by compaction.

Sponge spicules, common in the Upper Jurassic marine sandstones in the North Sea (Aase et al., 1996; Vagle et al., 1994), have apparently dissolved away leaving sand-grain sized circular pores in some samples (Fig. 9A and B).

4.3. Diagenetic minerals

The most common diagenetic constituents of the Tambar reservoir rocks found in the three wells are microcrystalline quartz (Fig. 10), illite and chlorite (Fig. 10C and D), quartz cement (Fig. 12), feldspar cement (Fig. 8B), dolomite and calcite (Fig. 13), and pyrite.

Calcite occurs in two forms: both as the early-formed, pore-occluding cement and as corrosive replacement of other minerals in minor amounts (<5%). In the early-formed calcite samples, the porosity and permeability are insignificant and other detrital grains have not undergone major dissolution or other mineral cement precipitation. The detrital grains appear to float in the large intergranular volume. The second is of a replacive type which occurs in minor amounts replacing detrital grains and clays.

Traces to minor amounts of pyrite are widespread in occurrence, sitting in pores and on grain surfaces, associated with micas and mud intra-clasts. Pyrite occurs as aggregates of small cubic crystals (<15 μm) or in the form of framboids.

Diagenetic feldspar occurs as K-feldspar or albite overgrowth. K-feldspar cement is a common authigenic mineral in most samples, the content of which ranges from 0 to 5% (2% on average) of the rock volume. Though the thickness of K-feldspar overgrowth reaches up to 15 μm, it mainly has undergone etching due to partial dissolution leaving most of the detrital feldspar grains intact (Fig. 8B). The albite and K-feldspar cements have been overgrown by chlorite and illite and also engulfed by quartz overgrowth that has developed on adjacent quartz grains. Feldspar cements therefore predate these mineral cements.

Randomly oriented microcrystalline quartz is the most abundant diagenetic mineral in the Tamar field reservoir. It occurs in two forms: both as isopachous rims covering the detrital grains and as fillings to intergranular pores. Generally, euhedral microcrystalline quartz (2 μm–5μm) ranges in volume from 0 to 13% (4.8% on average) (Table 1; Fig. 10). This amount of microcrystalline quartz is somewhat greater than that reported previously from sandstones worldwide (Aase et al., 1996; Jahren and Ramm, 2000; Ramm, 1992). The pore fillings occur as aggregates of prismatic euhedral quartz crystals similar in size to the grain coatings and are locally associated with fibrous illite and framboidal pyrite. The microcrystalline quartz is more associated with samples that contain sponge spicules (Fig. 9). In some places, there is some sort of coating between the sand grain surface and the microcrystalline quartz (Fig. 10D). This may be a layer of amorphous silica, analogous to that observed in the Heidelberg sandstone (French et al., 2012; Worden et al., 2012).

Illite is the most abundant clay mineral in the Tambar sandstone reservoir (accounting for 0-16% with an average of 4.3%). It is associated with highly altered feldspar and muscovite and can be interpreted to be a product of labile detrital grain alteration, e.g. detrital intra-clast alteration (Fig. 11C). Illite occurs as fibrous, hair-like radially-disposed crystal and filamentous crystal bridging pore throats (Fig. 11B) or filling pores (Fig. 11C). Illite can be identified from XRD analysis by the typical prominent peaks (10 Å).

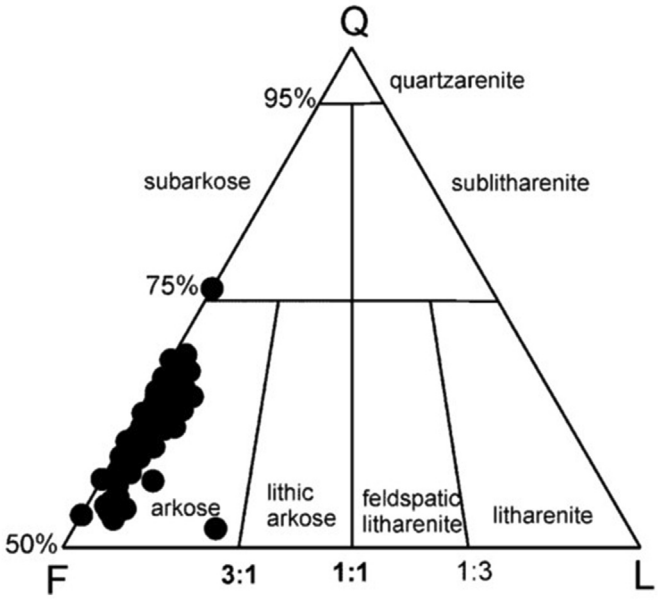

Fig. 6. Detrital composition of the Tambar reservoir sandstone samples plotted on the classification diagram (Folk, 1968) (the sandstones are exclusively arkoses).

Chlorite occurs as rare pore-filling aggregates. It consists of microcrystalline plates aligned perpendicular to the surface of detrital grains forming rosettes (Fig. 11D), and is often interwoven with illite and pore fillings of a flaky type. It is sometime seen clearly related to the decomposition of detrital feldspar and lithic grains. Chlorite is also identified from XRD analysis by the two typical prominent peaks (14 Å and 7 Å).

Quartz cement in the Tambar oil field occurs as overgrowth and, less commonly, as prismatic outgrowth. It has an average of 2% by volume across the field but locally abundant and pervasive completely blocking pores (Figs. 7D and 12). It is rare in the microcrystalline quartz coated samples. However, patches of quartz cements are locally found growing on top of the microcrystalline quartz. Microquartz refers to the smallest diagenetic crystal of quartz that grows in pores or around the detrital grains usually ranging from 0.5 μm to 10 μm (Vagle et al., 1994) and occurs with different crystallographic orientation to the host detrital grains (French et al., 2010; Haddad et al., 2006), while quartz overgrowth has a diameter ranging from greater than 20 μm (Vagle et al., 1994) to up to 100 μm (Aase et al., 1996), typically growing syntaxial to the substrate. In this study, crystals of greater than 20 μm are considered as quartz overgrowth. There is no clear relationship between quartz overgrowth abundance and depth where microquartz is not involved. The only substrate on which the authigenic quartz cement grows in the Tambar oil field is detrital quartz and feldspar. Overgrowths are typically 15 μm–30 μm thick with euhedral terminations although cutting effect may alter the true thickness. SEM-CL was used to look for zonation of the quartz cements (Hogg et al., 1992). No zonation is observed (Fig. 12), suggesting either continuous growth under constant water chemistry conditions and at a similar rate or one phase of growth. Quartz grain fracturing is apparent in some grains under CL examination (Fig. 12B). Quartz overgrowth encloses illite, chlorite and feldspar cements. Thin dust rims or fluid inclusions commonly separate the quartz overgrowth from the detrital grain.

Dolomite occurs as either rhombs of 100 μm–200 μm long growing into pores space, clusters of rhombs that have grown together to fill the pore space (Fig. 13) or a mineral pervasively

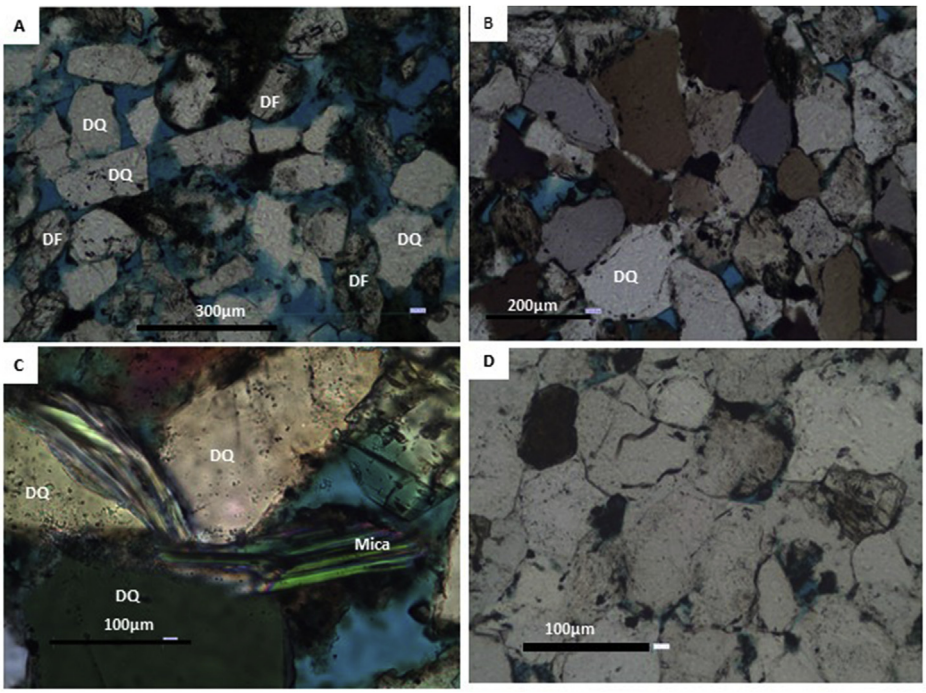

Fig. 7. Thin section images of detrital mineralogy. (A and B) Plane polarized light showing fine and coarse-grain texture and composition of the Tambar reservoir sandstones; (C) Crossed polarised quartz grains and mica deformed at grain contact; (D) Plane polarized light image showing quartz cemented part of the sandstone. Note: cement occludes porosity completely. Key: detrital quartz (DQ) detrital feldspar (DF).

Table 1
Average petrographic properties of the oil and water leg sandstones from the three wells studied in the Tambar oil field.

Detrital diagenetic components	1/3-9-ST2 oil leg n = 23	1/3-9-ST2 water leg n = 8	1/3-3 oil leg n = 5	1/3-3 water leg n = 9	2/1-10 water leg n = 20	Weighted Mean
Mono quartz	33.8	32.5	31.3	30.2	36.1	33.9
Poly quartz	3.6	4.3	2.8	2.1	2.8	3.1
K-feldspar	10.8	13.6	11.7	11.7	13.1	12.1
Plagioclase	12.9	11.7	12.2	15.0	11.1	12.3
Sedimantary RF	0.2	0.0	0.4	0.3	0.3	0.3
Igneous RF	0.5	0.0	0.6	0.6	0.9	0.5
Metamorphic RF	0.7	0.5	1.3	1.0	1.0	0.9
Muscovite	1.9	2.1	3.0	1.3	0.6	1.8
Heavy Minerals	0.1	0.0	0.2	0.2	0.0	0.1
Glauconite	0.1	0.1	0.1	0.1	0.1	0.1
Calcite PF	1.9	0.3	0.0	0.0	1.9	0.8
Calcite replacive	1.2	2.3	2.7	2.0	1.6	2.0
Dolomite PF	0.3	0.7	0.4	1.3	1.6	0.8
Dolomite replacive	2.6	2.7	4.0	2.0	1.9	2.3
Illite PF	2.6	2.0	0.8	1.2	0.7	1.3
Illite replacive	2.7	4.1	3.4	2.3	2.7	3.0
Chlorite PF	0.1	0.0	3.0	1.9	0.5	2.3
Chlorite replacive	0.3	0.0	0.4	0.1	0.6	0.3
Quartz cement	2.3	0.8	0.3	1.4	3.6	3.2
Microcrystalline quartz	5.2	9.5	8.0	4.4	2.6	4.8
K-feldspar cement	1.6	0.5	0.8	3.5	3.0	2.1
Albite cement	1.8	0.5	0.9	3.0	2.2	1.7
Pyrite	0.3	0.1	0.4	0.3	0.5	0.3
Hydrocarbon stain	0.3	0.1	0.1	0.3	0.1	0.2
Siderite	0.2	0.0	0.0	0.3	0.2	0.1
Intergranular porosity	9.5	9.1	9.8	8.7	6.8	8.8
Intragranular porosity	2.5	2.4	1.9	5.0	2.8	2.7
Total	100.0	100.0	100.0	100.0	100.0	100.0

replacing other minerals. Dolomite cement is commonly observed to be enclosing quartz and feldspar cements. Dolomite crystals commonly have a non-ferroan core and become increasingly ferroan towards their outer margins (Fig. 13C). In some cases, the non-ferroan cores look as if they are partially resorbed with rounded embayments, suggesting two distinct phases of dolomite development separated by a dolomite partial dissolution event.

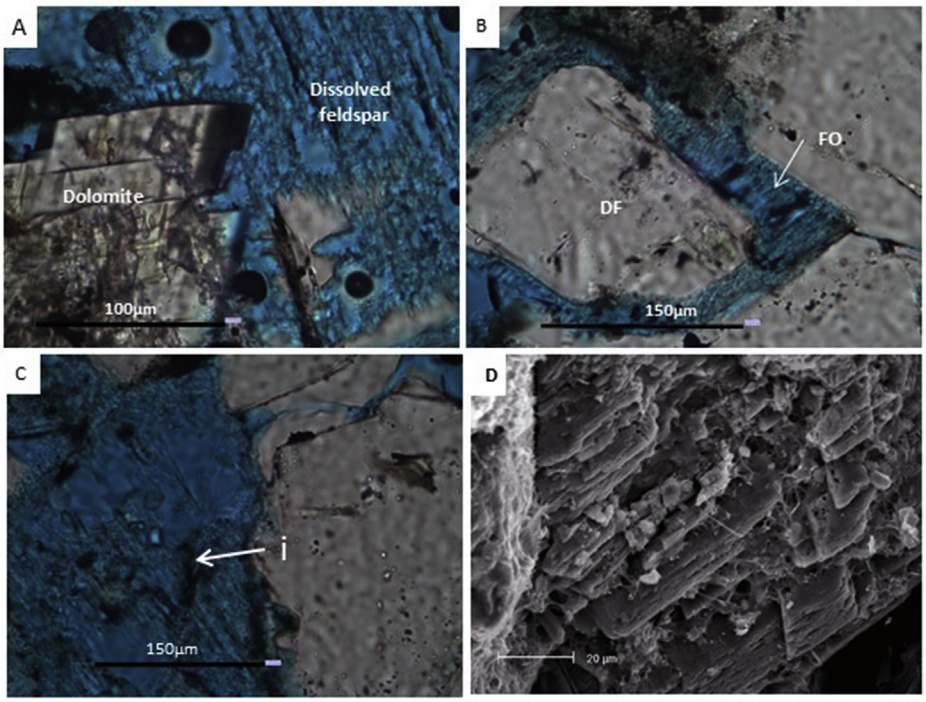

Fig. 8. Thin section images showing dolomite growing in secondary pores of detrital feldspar under dissolution (A), partially dissolved feldspar overgrowth (B), secondary pores under feldspar dissolution with traces of illite (i) (C), and SEM image showing feldspar decay (D).

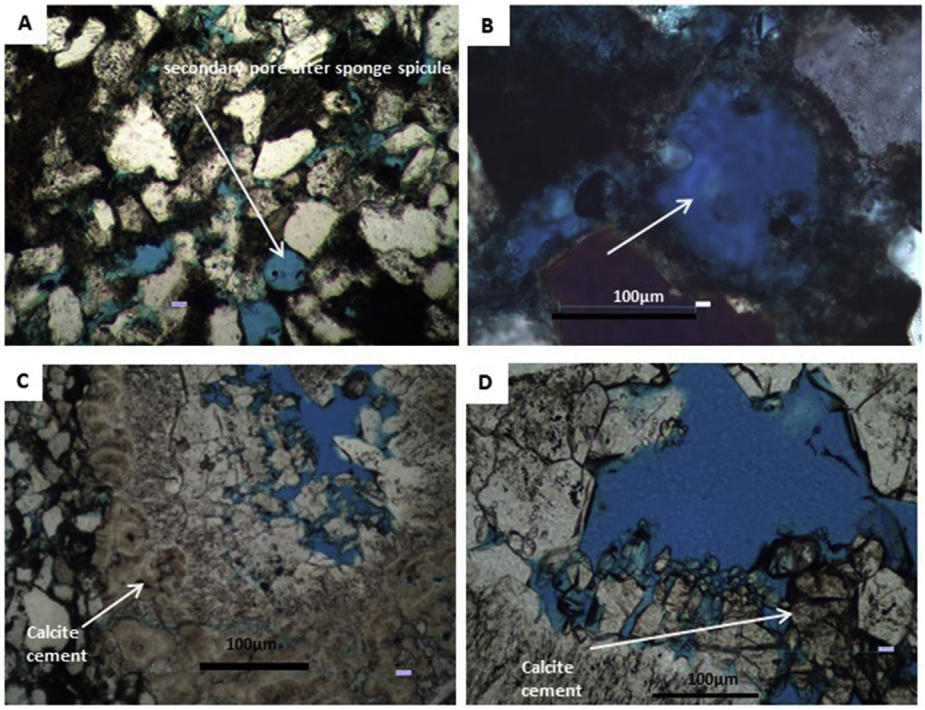

Fig. 9. Thin section images of secondary pores after sponge spicules dissolution (arrows) Note: A and B have the highest microquartz content among the samples.

4.4. Porosity and compaction

The porosity of the Tambar reservoir sandstone is of both primary intergranular and secondary dissolution types of varying sizes. The (total) porosity value from core analysis varies from 5% to 26% with an average of 14% for the Ula Formation from Tambar. Point count intergranular porosity is up to 16% and the moldic porosity is up to 7%. Moldic porosity has developed by partial or total dissolution of coarse and fine grains of detrital feldspar, sponge spicules, rock fragments, detrital mud and feldspar cements. Dissolved mica grains locally show intragranular porosity and get expanded into open pores making pseudomatrix. The

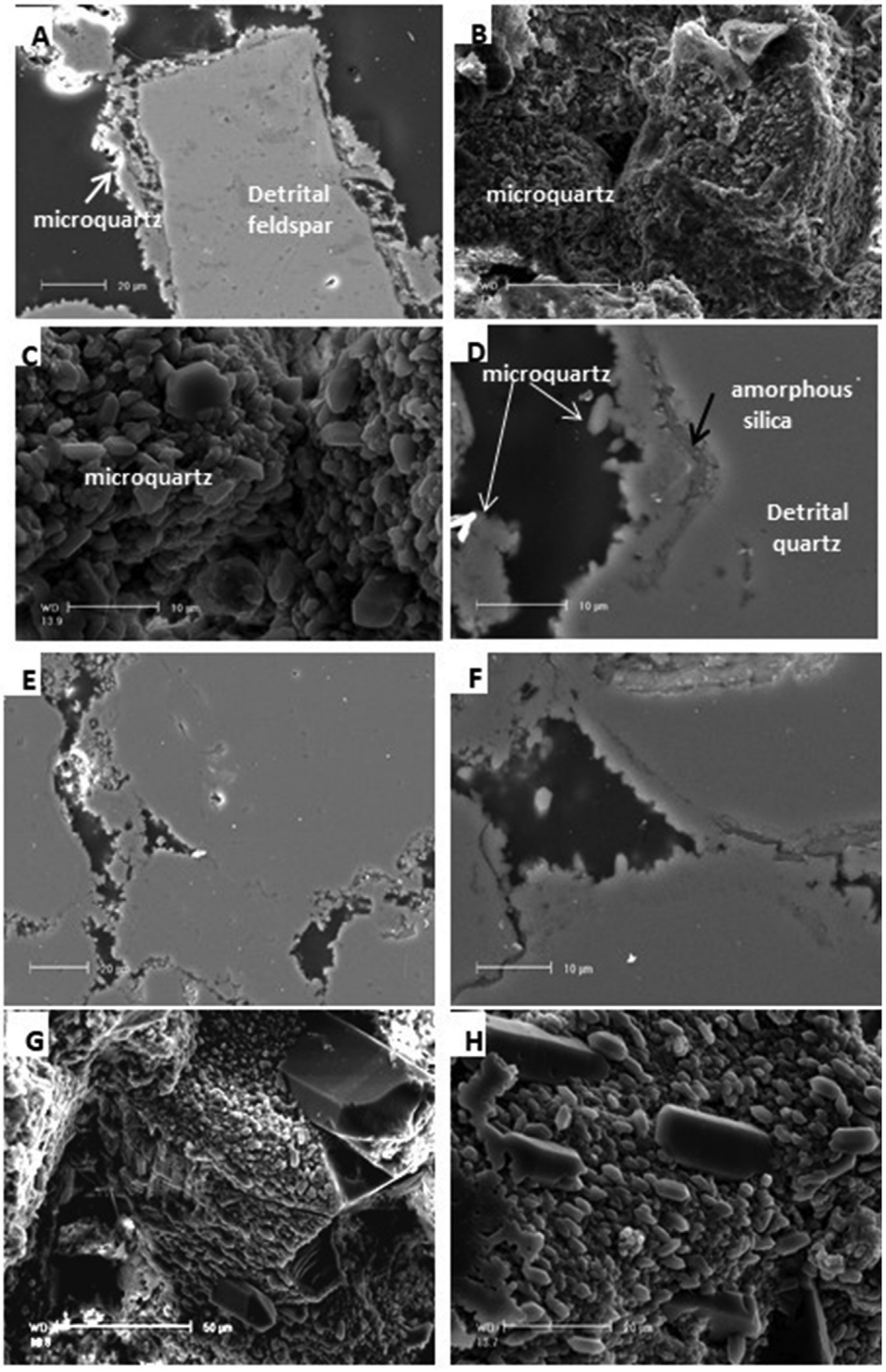

Fig. 10. SEM images of grain-coating microcrystalline quartz cement (A), grain rimming microquartz around feldspar grain (B), thick grain-coating microquartz (C), high magnification view of prismatic microquartz crystals coating grain surface in highly porous units of the reservoir (D), grain rimming microquartz around detrital quartz grain within layer of amorphous silica (black arrow) between them (E), pore-filling microquartz (F), grain rimming and pore-filling microquartz (G, H), high magnification view of microquartz with patch of quartz cement growing. It is not known whether quartz cement is growing in areas with no microquartz or in a fracture. Note the lack of significant quartz overgrowth in all the microquartz coated samples.

primary pores are affected by compaction and precipitation of authigenic quartz cements and clays. Evidence of mechanical compaction can be seen from the bending of mica grains (Fig. 7C), deformation of mud intraclasts and grain re-arrangement with straight grain contacts. Secondary porosity due to dissolution of feldspar grains and cements contributes significantly to the overall porosity and pore connectivity of the sandstone (Fig. 8). Pressure solution (chemical compaction) can be observed at long sutured contacts between sand grains.

4.5. Fluid inclusion thermometry and petrology

Microthermometric studies on fluid inclusions were carried out on ten samples. The inclusions are generally small ranging from 4 μm to 15 μm at a vapour-to-liquid ratio of 1:10 to 1:4. Only fluid inclusions within quartz cements and at quartz cement-quartz grain boundaries were measured.

Both aqueous and petroleum inclusions were found. All aqueous inclusions contain two phases (liquid and vapour) and display homogenization temperatures between 120 °C and 168 °C (Fig. 14). The aqueous inclusions are unimodal and mainly homogenized between 150 °C and 160 °C. Oil inclusions were found in three out of ten samples, relatively rare even in these samples. The oil inclusions show a lower homogenization temperature (from 120 °C to 145 °C) compared with aqueous inclusions. Given the last ice melting temperature, the formation water salinity for the Tambar reservoir sandstone ranges from 0.5 wt % to 18 wt % NaCl equivalent (Fig. 15) which is much higher than the salinity of the (marine) waters in which these were deposited (3.5 wt % NaCl).

4.6. Stable isotope geochemistry

The $\delta^{18}O$ values of dolomite cement in the Tambar sandstone reservoir range from −11.77‰ to −3.57‰ PDB. There is a clear differentiation between oil and water leg samples, with the most depleted values in the water leg (Fig. 16A and B; Table 2).

The $\delta^{13}C$ values of the dolomite cement range from −0.7‰ to −1.12‰ PDB, with the most negative values from the high water-saturation parts of the cored sections (Fig. 16A).

The present-day formation water from nearby Ula Field (of the same reservoir age, the same detrital mineralogy, the same stratigraphy, similar thermal and filling history) has a $\delta^{18}O$ value of 3.26‰ V-SMOW. If Ula and Tambar are assumed to have the same type of formation water, then it is possible to derive the temperature of dolomite growth using the appropriate isotope fractionation equations (Fig. 17) (Land, 1983; O'Neil and Epstein, 1966). Dolomite in the water leg has grown, or been recrystallized, at a temperature close to the present while dolomite in the oil leg appears to have grown at a significantly lower temperature, possibly before oil entered the reservoir (Fig. 16C).

5. Discussion

5.1. The most significant diagenetic mineral cements and processes in the Ula Formation, Tambar

The petrographic (point count) data show that the most volumetrically-important cement is microcrystalline quartz (accounting for 4.8%) (Table 1). Quartz cement is the next most important mineral (accounting for 3.2%). There are approximately equal volumes of albite, K-feldspar and pore-filling illite cements on average (all close to an overall value of 2% on average). There are small but highly variable amounts of pore-filling dolomite (accounting for 0.6%). Calcite either tends to be absent or totally occludes pores (representing 45% of the total rock volume). These average values mask a wide range in some of the cements;

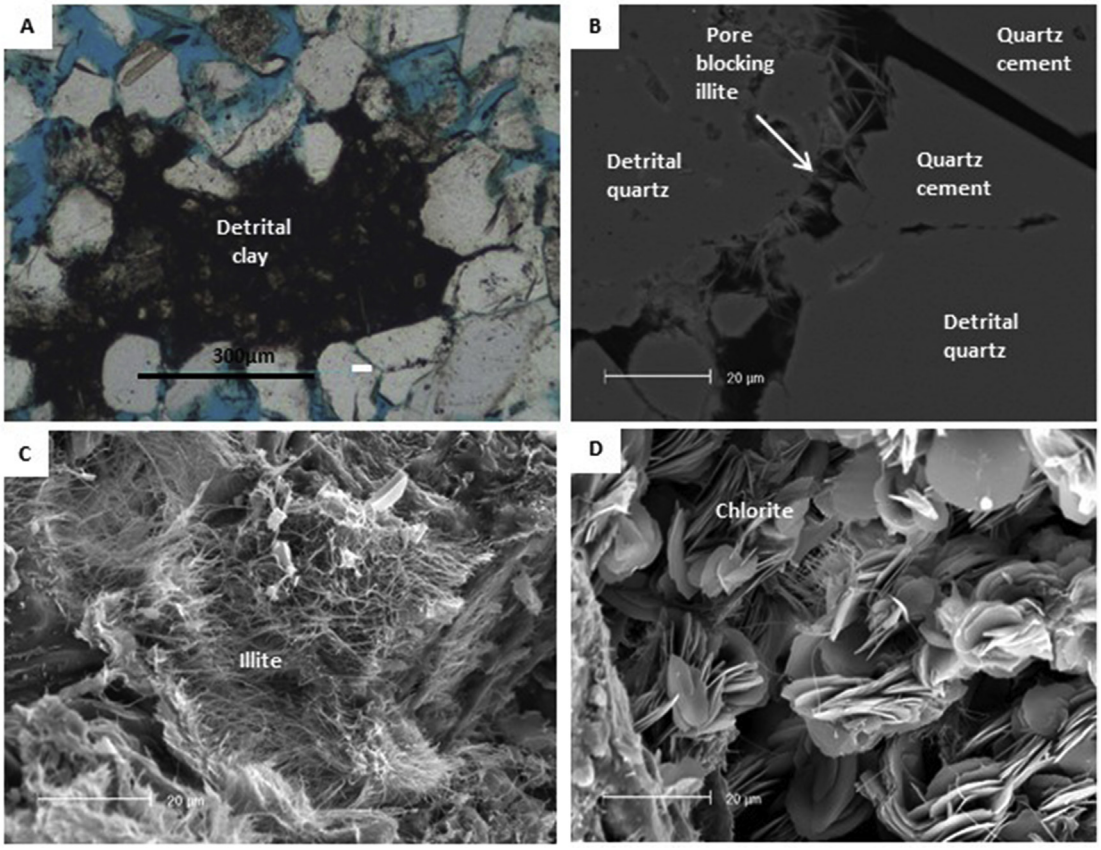

Fig. 11. Thin section and SEM images of detrital clay and illite and chlorite cement (A), detrital clay matrix (B); and the SEM images showing pore throat blocking illite (C), high magnification view of pore-filling fibrous illite (D), and high magnification view of pore-filling chlorite. The pore-filling clays have no significant effect on porosity but can reduce permeability considerably.

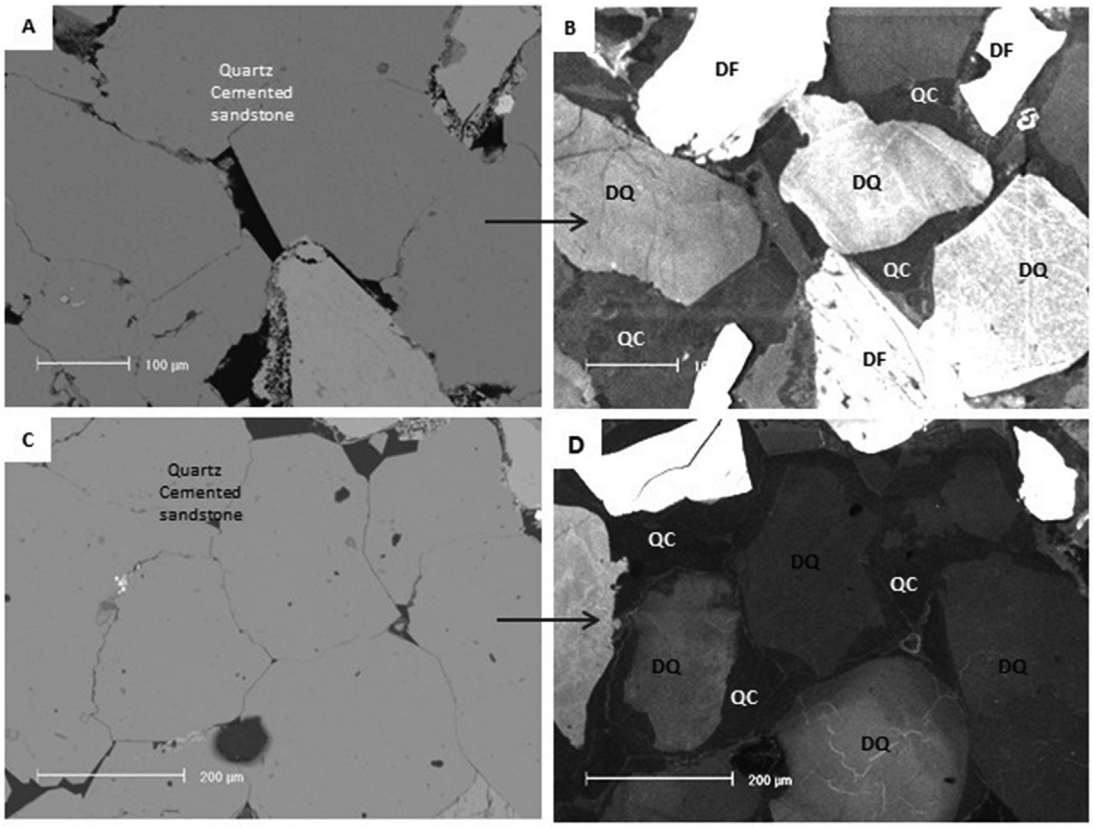

Fig. 12. BSEM and SEM-CL images of quartz cemented sandstone (A and C), BSEM images of quartz cemented sandstone (B and D), and CL images distinguishing detrital quartz and authigenic quartz cement (same as A and C). Key: detrital quartz (DQ); detrital feldspar (DF); feldspar cement (FC); quartz cements (QC).

especially quartz cement which can occupy up to 16% by volume. There are also trace quantities of chlorite and pyrite.

Intergranular volumes have been derived from the point count data and Houseknecht-type diagrams have been plotted with the data subdivided by grain size and water saturation. All samples, however, they are split, fall into the cementation-dominated portion of the diagram with cementation clearly dominating over compaction as the main control on porosity-loss (Fig. 18). There are no clear differences in the porosity-loss behaviour of the finest- and the coarsest-grained sandstones from the Ula Formation in Tambar.

It is unusual for the sandstones from the Tambar oil field containing such a large volume of microcrystalline quartz. In many Upper Jurassic sandstones from the North Sea Basins, microquartz is present as a very thin grain-coating mineral representing a fraction of a percent of overall rock volume (Aase et al., 1996; Ramm et al., 1997). The mean of 4.8% in Tambar oil field reported here is a clear exception.

5.2. Sequence of mineral growth

By examining the petrographic images collected using light optics, SEI, BSEM and SEM-CL, we are likely to deduce an overall order of mineral growth based on contacts and enclosures (Fig. 13D), which is represented in a paragenetic sequence (Fig. 19).

Early diagenetic/eodiagenetic cements, probably related to the marine environment of deposition, include glauconite, pyrite and calcitepossibly. These tend to be volumetrically minor and do not play much of a role in controlling reservoir quality. However, calcite is dominant in some samples filling all intergranular volume and leaving a floating grain texture.

A fall in relative sea level likely leads to a meteoric water influx with marine pore-waters flushed through the sandstone by low salinity water (Morad et al., 2010). This in turn leads to the onset of dissolution of feldspar grains initiated at the later part of eodiagenesis and continues to mesodiagenesis evidenced by secondary intragranular pores. Microcrystalline quartz growth typically starts to happen during the eodiagenesis and is at an advanced stage by the time sandstones are buried to about 60 °C. Microcrystalline quartz growth thus straddles the conventionally-assumed boundary between the eodiagenesis and mesodiagenesis (Worden and Burley, 2003).

Mesodiagenesis/burial diagenesis involves the following events in sequence: feldspar dissolution, K-feldspar and albite cementation, and chlorite, illite, quartz and dolomite recrytallization. There is almost certainly some degree of overlap between some of these cements in growth although spatial separation of growth sites makes unequivocal determination of the exact relative start and end times of cementation rather difficult. Feldspar cementation may have started in the early diagenesis regime (Bjorlykke et al., 1988) and possibly continued during the initial stages of mesodiagenesis. Feldspar dissolution may also have started relatively early but continued through to burial diagenesis as revealed by the dissolution of K-feldspar cement after quartz cementation (Fig. 8B) as well as secondary pores developed within feldspars containing illite cement (Fig. 8C and D). Illite and chlorite growth, the latter being largely irrelevant to reservoir quality, occurred at approximately the same time and overlapped with the feldspar cementation and development of microcrystalline quartz coatings. Dolomite seems to have had two growth episodes: one relatively earlier during the mesodiagenesis and one probably during the

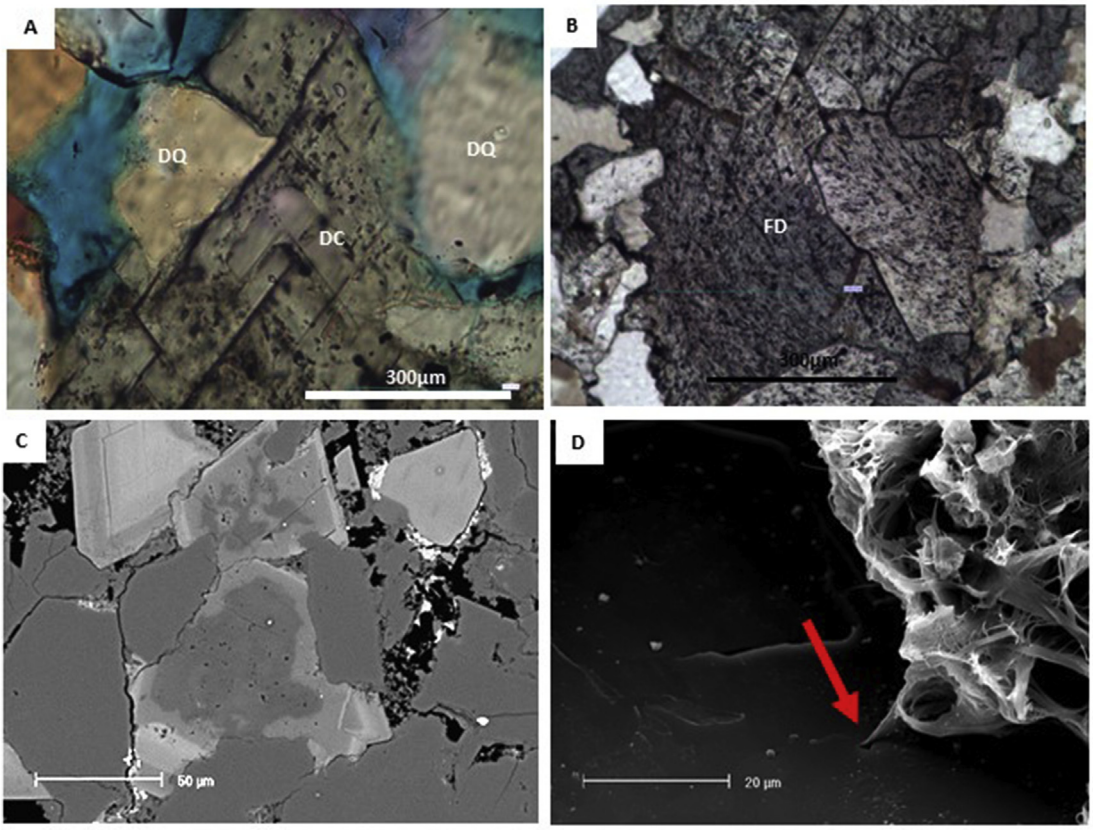

Fig. 13. Thin section images of dolomite cements. (A) Plane polar image of replacive dolomite cement; (B) Late ferroan dolomite replacing grains and cements (C); SEM image showing the zonationof dolomite cement becoming more ferroan toward the outer edge; (D) SEM image showing quartz overgrowth enclosing illite.

telodiagenetic stage. The simple interpretation of the oxygen isotope data corroborates (Fig. 16C) with the main growth of dolomite found in the oil leg occurring at about 80 °C–90 °C and the dominant phase of dolomite growth or recrystallization in the water leg occurring at about 145 °C–160 °C. Dolomite cement becomes increasingly Fe-rich as diagenesis progresses. The relative lack of oil inclusions within quartz cement suggests that much quartz cementation occurred before oil-charging started. The few oil inclusions found in the three out of ten fluid inclusion wafers suggest that oil-charging happened towards the end of quartz cementation. The differences in the carbon and oxygen isotope values of the dolomite above and below the oil-water contact (Table 2; Figs. 16 and 17) suggest that oil-charging had a major impact on dolomite diagenesis.

The aqueous inclusions from quartz cements show a minimum temperature of about 130 °C with a mode of about 140 °C–150 °C (Fig. 14). This represents an unusually high minimum temperature for quartz cementation, conventionally assumed to commence at about 80 °C–100 °C and reaching its apogee at about 120 °C (Walderhaug, 1994; Walderhaug et al., 2000). Given the thermal history (Fig. 3), it is possible to conclude that quartz cementation started at about 30Ma. The high initiation temperature suggests something has inhibited quartz cement growth.

5.3. Sources of mineral cements

Eogenesis (early diagenesis) has been defined as those processes that occur when sediment is close to the surface and in communication with surface-supplied oxygenated water (Burley, 1984), equivalent to a burial depth of <2000 m and a temperature of <70 °C. Calcite and pyrite are early diagenetic cements in the Ula Formation in Tambar. Calcite tends to totally block porosity where present (accounting for 45% of the rock in volume) and thereby grows before any significant compaction occurs. Bioclastic fragments are present in a few samples suggesting that the calcite cement was sourced by dissolution and reprecipitation of shelly material co-deposited with the sediment. Pyrite cement is very common is marine sandstones. It occurs as framboids, typically of a bacterial sulphate reduction origin but is also locally recrystallized into clusters of bipyramidal (euhedral) crystals. The sulphide would be probably sourced from reduced marine aqueous sulphate and the iron probably supplied by the clastic sediments.

Microcrystalline quartz is a relatively early diagenetic mineral that coats sand grain surfaces (quartz grains and feldspar grains alike) (Fig. 10A, D) and would be probably supplied by the dissolution of amorphous silica sponge spicules. The Upper Jurassic sponges are siliceous (i.e., composed of amorphous opaline silica) and their bioclastic fragments tend to be composed of sand-grade material. The Upper Jurassic marine sandstones in the North Sea Basins commonly contained sponge spicules when they were deposited (Aase et al., 1996; Aase and Walderhaug, 2005; Jahren and Ramm, 2000; Ramm, 1992; Ramm et al., 1997; Stokkendal et al., 2009; Vagle et al., 1994; Weibel et al., 2010). There are sand grain-sized dissolution voids (secondary pores) in the Ula Formation in Tambar that are surrounded by microcrystalline quartz which are almost certainly the remnants of these spicules (Fig. 9A and B). There are also pores filled with clumps of microcrystalline quartz crystals (containing microporosity) that may represent the

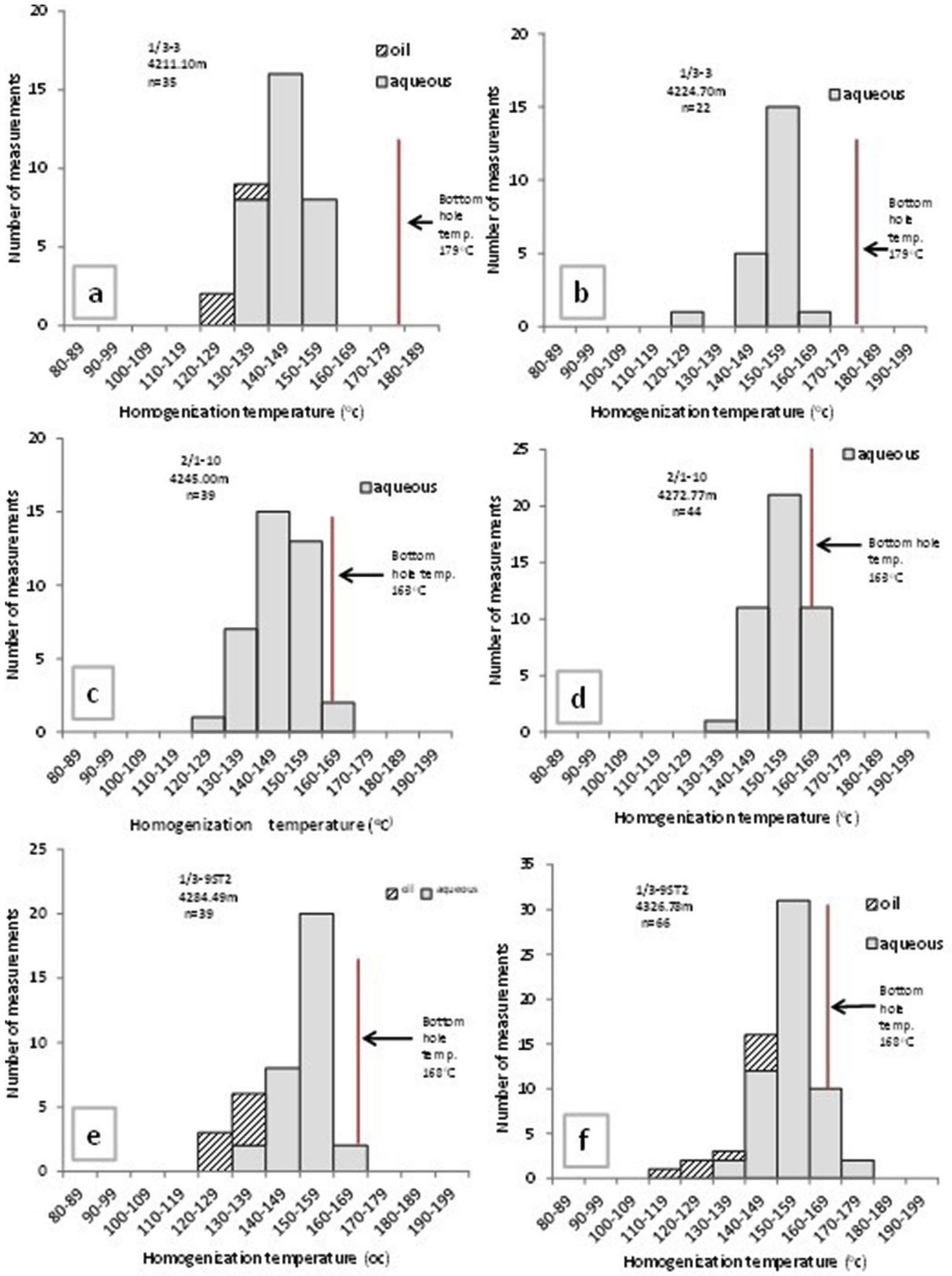

Fig. 14. Histograms showing fluid inclusion homogenizarion temperatures measured at different depths for the oil and aquous inclusions in quartz cement and the interface between quartz grain and cement. The red vertical line shows the measured bottom hole temperatures. Well name, inclusion depth and number of measured inclusions are shown for each histogram.

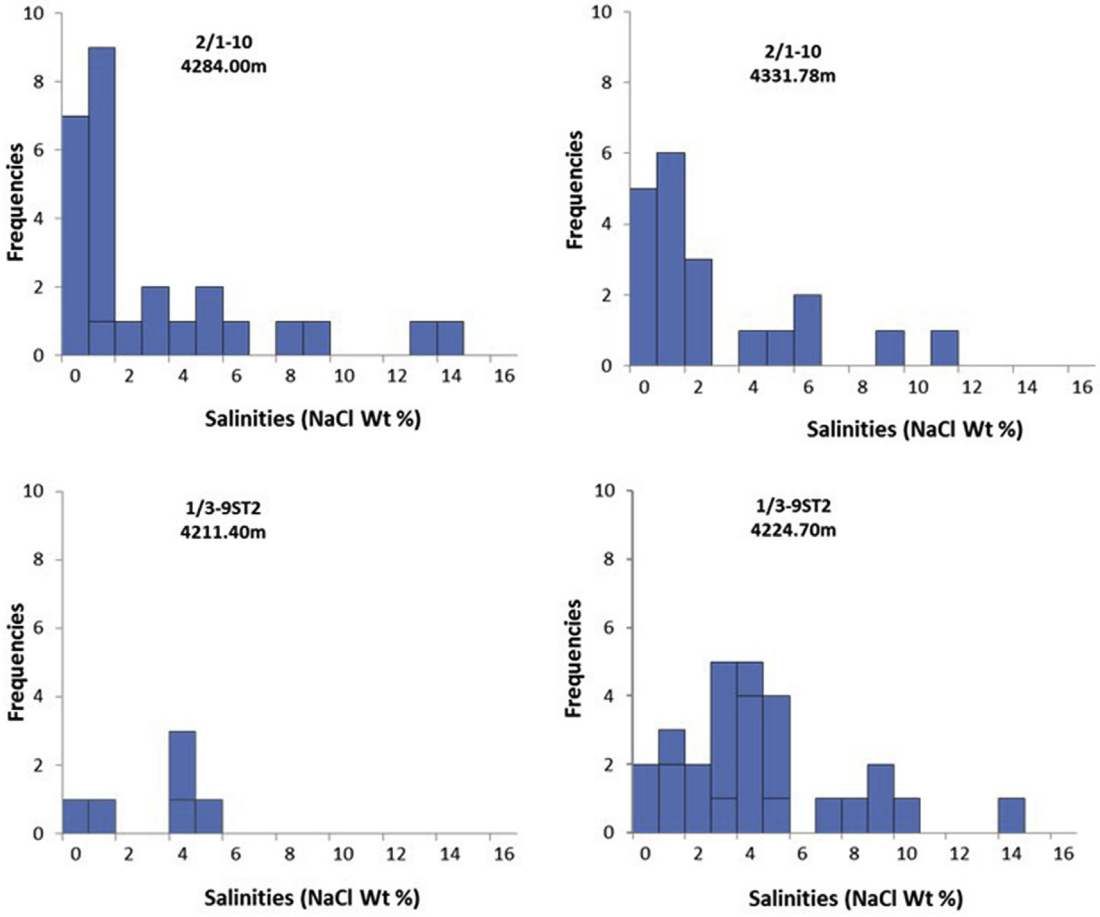

Fig. 15. Fluid inclusion salinity plots with data derived from last ice melting temperatures from aqueous inclusions within quartz cement.

remnants of recrystallized sponge spicules. The generalised diagenetic sequence of amorphous silica diagenesis is: opal-A (biogenic silica) transforms to disordered opal-TC, which in turn transforms to ordered opal-CT and cryptocrystalline quartz or chalcedony which then finally is replaced by microcrystalline quartz (Williams and Crerar, 1985; Williams et al., 1985). The presence of a potentially amorphous silica film of <1 μm between microcrystalline quartz crystal and detrital quartz grains (Fig. 10D) suggests that the Tambar reservoir sandstone followed this process with the amorphous silica being supplied by sponge spicule dissolution and local reprecipitation.

Feldspar cement would be likely sourced by reactions involving the large volume of detrital feldspars. Feldspar-feldspar pressure solution may have occurred as might simple dissolution of metastable forms of feldspar (in terms of crystallography and/or mineral chemistry) followed by the growth of more stable forms of feldspar (Schmid et al., 2004). Pore-filling and replacive illite cements, and the less volumetrically-significant chlorite, grew before quartz and overlapped with feldspar and microcrystalline quartz. Illite would be probably sourced from feldspar alteration reactions (Barclay and Worden, 2000; Worden and Morad, 2003). The source of chlorite is not certain but it may have been generated by the alteration of pre-existing Fe minerals (i.e., pyrite and glauconite).

Dolomite cement has a range of $\delta^{13}C$ values (Fig. 16A). The high values are similar to those of the Jurassic marine bioclastic carbonates (Veizer et al., 1999) suggesting that the dolomite is at least partly the result of dissolution and precipitation of primary bioclastic grains. The low values suggest that there has been an influx of diagenetically light carbon during the diagenesis. Note that the high $\delta^{13}C$ values correspond to a lower temperature growth compared with the low $\delta^{13}C$ values (Fig. 16C), as interpreted from the dolomite $\delta^{18}O$ values. The pattern of evolution to progressively lower $\delta^{13}C$ values at progressively higher diagenetic temperatures is commonly reported. There are a number of possible sources of isotopically light carbon during deep burial diagenesis with the most likely being CO_2 (or organic acid precursors) derived from petroleum source rocks (Macaulay et al., 1998). The distribution of $\delta^{13}C$ values (high in the oil leg, lower in the water leg) suggests that the supply of isotopically-distinct carbonate after oil emplacement was inhibited in the oil leg relative to the water leg. Table 3 also suggests that oil leg samples have less pore-filling dolomite than water leg samples.

Quartz cement, in many deeply buried sandstones the most volumetrically important cement, has a number of potential sources (Kraishan et al., 2000). The growth of quartz cement commences at relatively high temperatures (Fig. 14) suggesting that such smectite alteration reactions are not important. Some quartz cement may have been sourced by pressure solution, although intergranular volumes and porosity-loss are controlled by cementation instead of compaction (Fig. 18) and stylolites are not common features of these sandstones even if long and sutured interpenetrating grain (micro-stylolites) contacts are present. Quartz grains have flattened margins against mica flakes suggesting minor local quartz dissolution (Oelkers et al., 1996). Feldspar decay reactions may have contributed to the supply of silica. Quartz cement may have been sourced partly by the dissolution and

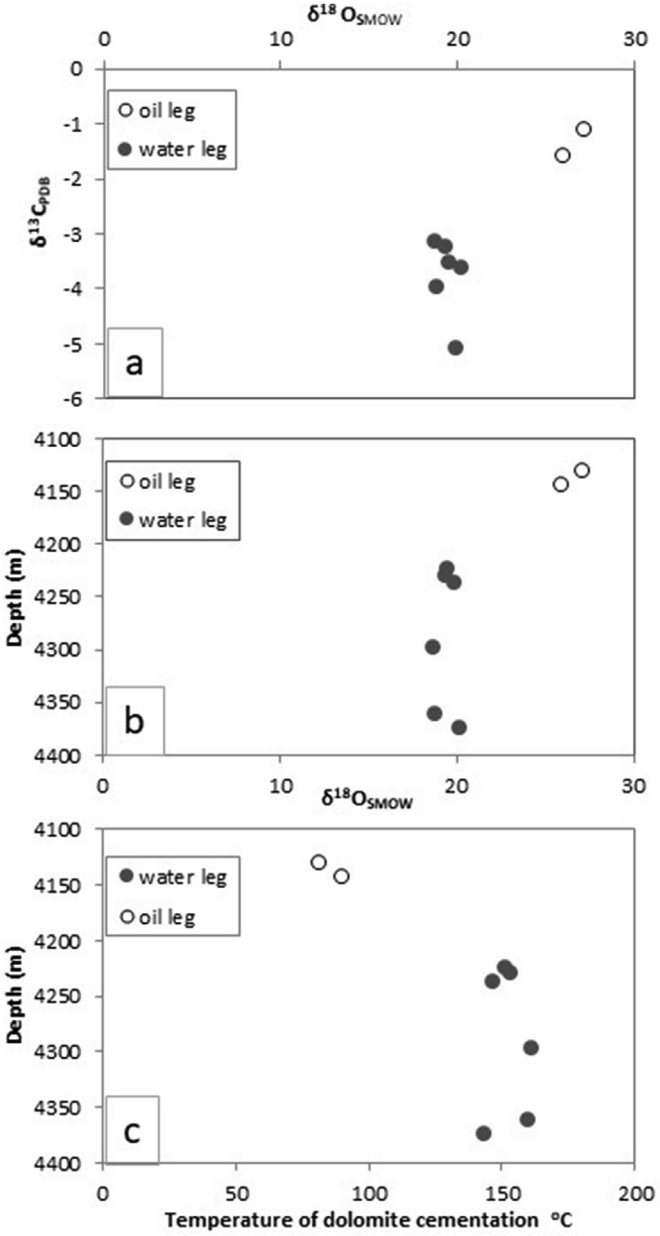

Fig. 16. (A) Carbon versus oxygen isotope plot for the dolomite in the Tambar rservoir sandstone; (B) Oxygen isotope of the dolomite vs. depth with data split by oil leg and water leg samples; (C) Interpreted temperature of growth for the dolomite in the oil leg and the water leg assuming that the formation water at the time had the same $\delta^{18}O$ as present-day formation water (3.2‰ V-SMOW).

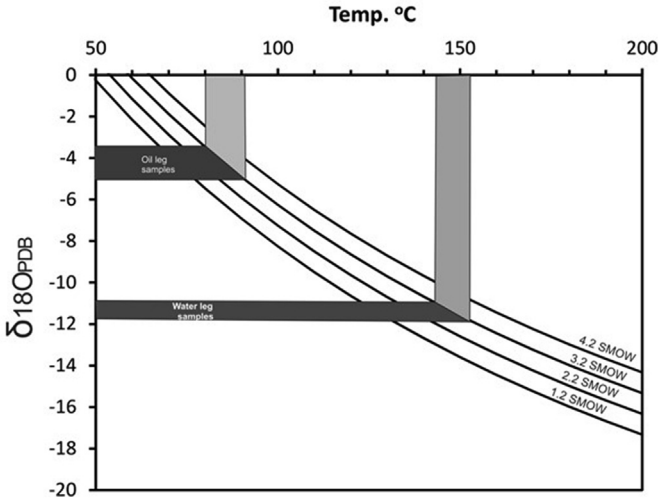

Fig. 17. Curves showing the relationship between the $\delta^{18}O$ values of diagenetic dolomite, reflecting possible temperatures of the dolomite precipitation. The vertical bars show the range of temperatures for samples in water leg and samples in oil leg. Estimated local marine water composition is 3.2‰ SMOW. The curves define the range of possible water compositions from which the dolomite could have been precipitated.

reprecipitation of more fine-grained forms of quartz through an Ostwald ripening process (Chang and Yortsos, 1994), for example, the spongey masses of microcrystalline quartz that are so common in these sandstones (Fig. 10D).

5.4. Main controls on reservoir quality

Reservoir quality includes porosity and permeability as defined by conventional core analysis techniques (Fig. 20). The range of helium-derived porosity values of these sandstones is good (an average of 16.1% for all samples in the petrological study). However, the permeability values are rather poor (with an arithmetic mean of 38mD, geometric mean of 4mD).

The diagrams of intergranular volume (IGV) vs. the volume of pore-filling cements (also known as Houseknecht diagrams) (Fig. 18), demonstrate that the Ula Formation in Tambar is cementation, as opposed to compaction, dominated. These rocks have undergone relatively little compaction but much cementation by microcrystalline quartz, quartz overgrowth, illite, dolomite, albite, K-feldspar, etc.

In essence then, these sandstones have retained fairly good porosity even at a burial depth of >4000 m and temperatures in excess of 160 °C, since they have undergone relatively little compaction (Fig. 18). However, they do not have especially good permeability. The controls on reservoir quality are examined in detail as follows.

Table 2
Dolomite isotopic composition of the Tambar field reservoir sandstones.

$\delta^{13}O_{dol}$PDB	$\delta^{18}O_{dol}$ SMOW	δ^{18}Owater SNOW (after Warren et al., 1994)	Interpreted tempreture of growth T°K	Interpreted tempreture of growth T°C	$\delta^{13}CV_{PDB}$	Depth	Fluid
-3.57	27.18	3.26	354.8	81080	-1.12	4131.5	oil
-4.72	26.00	3.26	363.36	90.36	-1.61	4144.1	oil
-11.01	19.51	3.26	424.56	151.56	-3.52	4224.1	water
-11.15	19.36	3.26	426.38	153.38	-3.23	4229.7	water
-10.63	19.91	3.26	419.92	146.92	-5.07	4237	water
-11.77	18.73	3.26	434.25	161.25	-3.16	4297.49	water
-11.66	18.84	3.26	432.87	159.87	-3.96	4361.5	water
-10.35	20.19	3.26	416.66	143.66	-3.63	4373.65	water

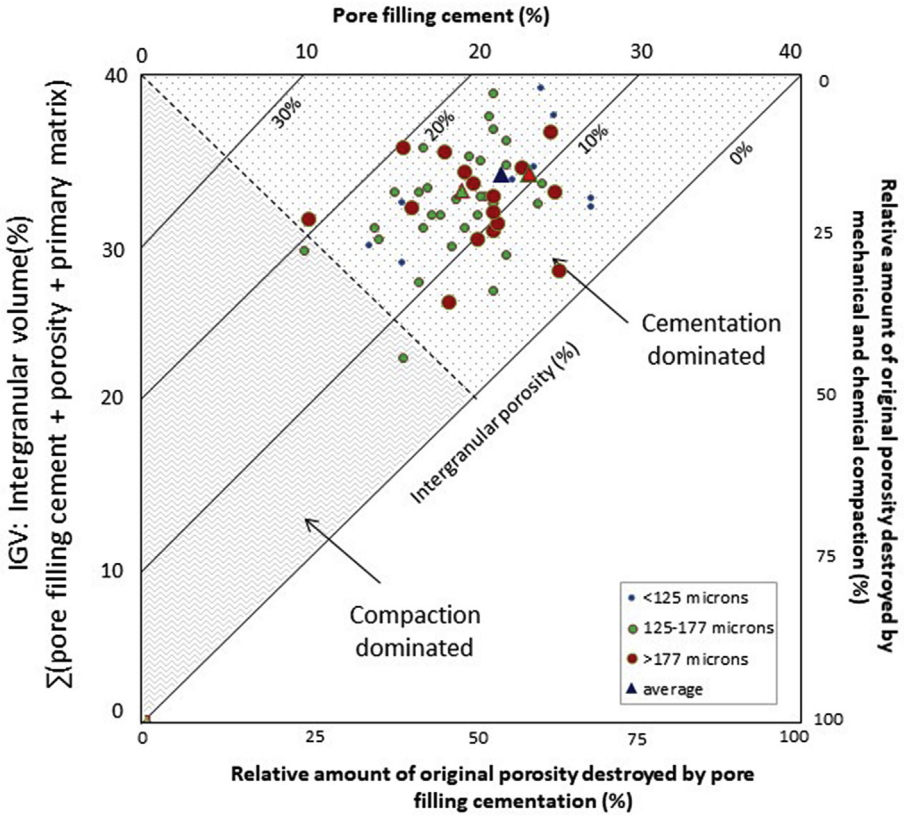

Fig. 18. Houseknecht-type plots' data split by grain size of sandstone. There is no clear separation in porosity loss between samples of different grain size.

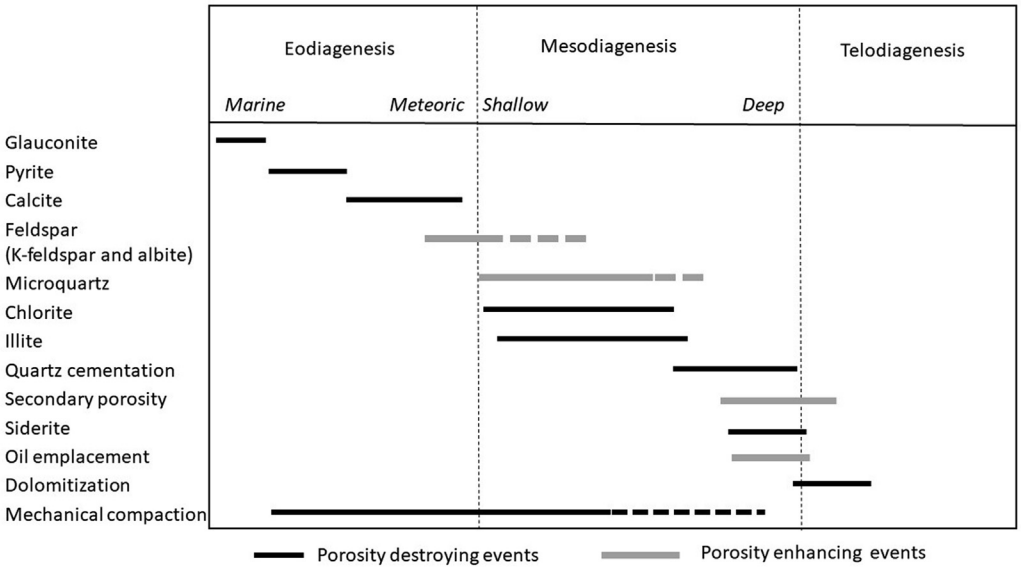

Fig. 19. Simplified paragenetic sequence of the diagenetic processes in the Tambar reservoir sandstones. Eogenetic processes include the formation of calcite, pyrite and dissolution of feldspars. Mesogenetic events include precipitation of microquartz, illite, chlorite quartz overgrowth and ferroan dolomite.

Grain size can have an important effect on permeability since small grains lead to narrow pore throats (Bryant et al., 1993; Cade et al., 1994; Evans et al., 1997). The data from Tambar have been subdivided by depositional grain size into three classes (<125 μm (very-fine), 125-177 μm (lower fine) and >177 μm (upper fine)) and plotted on separate conventional linear porosity-log permeability diagrams (Fig. 20A) revealing that there is a subtle separation of the grain size classes. The coarser sandstones are plotted to the left of the finer-grained sandstones, so they seem to have a slightly higher permeability for a given porosity compared with the finer-grained sandstones. It is also noteworthy that the 125 μm –177 μm grain size class (lower fine sand) has a cluster of points at >100mD suggesting that the very best reservoir quality is found in these lower fine sandstones. Sorting does not seem to play a major role in

Table 3
Summary of reservoir quality indicators and controls for the three different grain size classes split into oil and water leg. Number of each grain size class: <125 μm oil (n = 9), water (n = 2); 125-177 μm oil (n = 13), water (n = 20); >177 μm oil (n = 6), water (n = 10).

Parameters	Fluid type	<125 μm grain size	125-177 μm grain size	>177 μm grain size
Core permeability (mD)	Oil	26.0	92.9	10.9
	Water	0.2	39.1	9.2
Core porosity (%)	Oil	18.0	19.1	11.7
	Water	13.0	18.7	9.0
Quartz cement (%)	Oil	0.1	2.0	7.9
	Water	0.8	0.9	9.2
Detrital clay (%)	Oil	6.5	5.9	2.5
	Water	7.6	4.9	1.8
Microcrystalline (%)	Oil	7.2	5.8	3.7
	Water	8.5	5.8	0.4
Dolomite (%)	Oil	4.7	1.3	0.6
	Water	3.5	2.9	2.7
Feldspar (%)	Oil	1.6	3.3	5.6
	Water	1.25	4.2	6.4

defining porosity-permeability variations in the Ula Formation in Tambar (Fig. 20B).

The total amount of clay minerals in sandstones can have a major effect on sandstone reservoir quality with more clay usually having a relatively small effect on porosity but a major detrimental effect on permeability (Worden and Morad, 2003). The core data have been subdivided on the basis of a total clay content of <4%, 4%–8% and >8%. The least clay-rich sandstones are plotted to the left of the diagram, so they seem to have a higher permeability (Fig. 20C). Porosity-permeability data have thus been divided on the basis of a quartz cement of less than and greater than 5% (Fig. 20D). The quartz cement-rich sandstones are plotted to the left of the diagram, so they seem to have a slightly higher permeability for a given porosity compared with the sandstones hardly containing any quartz cements.

Microcrystalline quartz is the most volumetrically important of

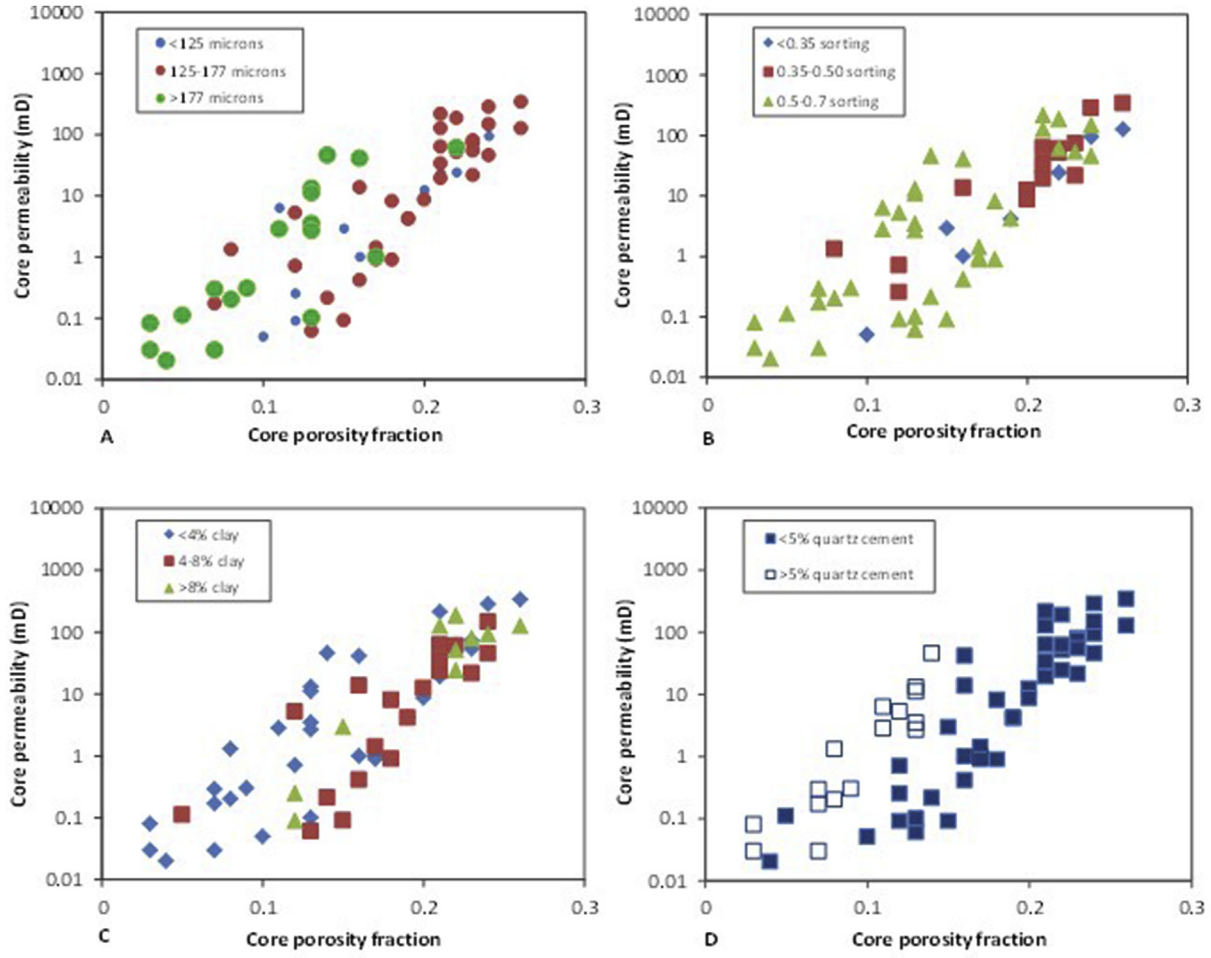

Fig. 20. Core analysis porosity vs. permeability of the Ula Formation in the Tambar oil field split by grain size ranges (A), split by degree of grain sorting (B), split by clay content (C), and split by the amount of quartz overgrowth (D). These show that the grain size class of 125 μm–177μm has a higher porosity and permeability.

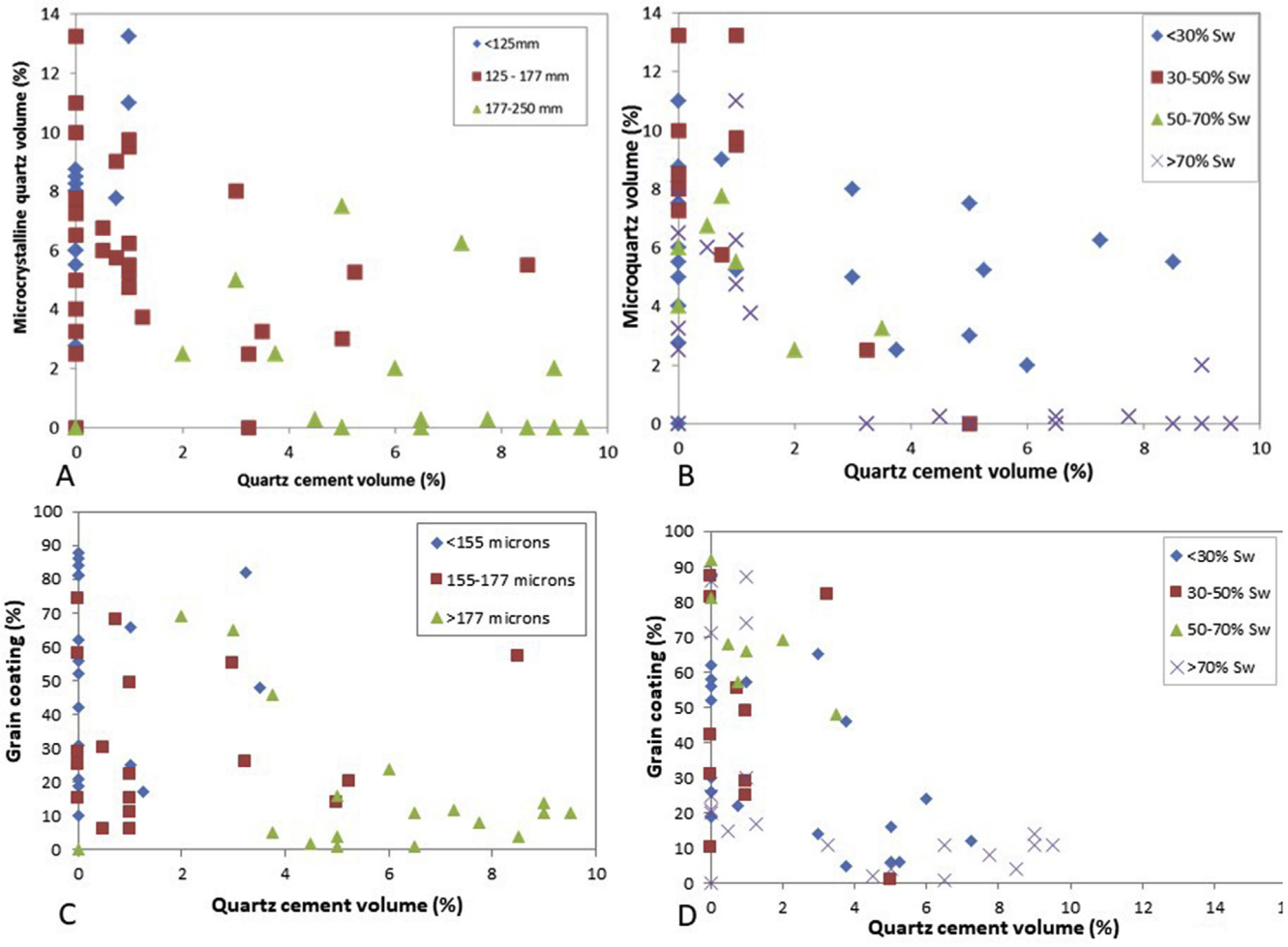

Fig. 21. Quartz cement volume vs. the amount of microcrystalline quartz split by grain size class (A), and split by calculated water saturation (B). Quartz cement volume vs. grain coating of microcrystalline quartz area split by grain size (C), and split by water saturation (D). Higher microquartz volume and grain coating show low quartz cement volume.

all the cements in Tambar. The core analysis data have been subdivided on the basis of the amount of microcrystalline quartz cements. The core analysis data do not split in any discernible pattern on the basis of the amount of microcrystalline quartz. To further investigate the relationship between quartz cement and water saturation, the petrographic and wireline data have been combined plotting quartz cement volume vs. microcrystalline cement volume with data split first by grain size and then water saturation (Fig. 21A and B). In addition, as for the absolute amount of microcrystalline quartz, it is possible to plot the average degree of grain coating by microcrystalline quartz (that is, what percentages of grains have a coating of the microcrystalline quartz in each sample) (Fig. 21C and D). Quartz cement is the most abundant in coarser sandstones (upper fine class) with the highest water saturation. Where more than 50% sand grains have been coated with microcrystalline quartz, the quartz cement volume is less than 4%. The degree to which grains are coated with microcrystalline quartz looks like a better diagnostic tool of the amount of quartz cement than the absolute quantity of microcrystalline quartz.

Dolomite cement is present in small amounts in most samples so that the core analysis data have been subdivided on the basis of a dolomite cement content of <1%, 1%–3%, and >3%. The samples with low and intermediate amounts of dolomite sit to the left of the data.

The effect of the addition of oil on diagenesis remains controversial (Bjørkum et al., 1998; Bloch et al., 2002; Worden et al., 1998). The timing of oil emplacement relative to the time of diagenesis is crucially important though seldom recognized (Molenaar et al., 2007). To test the role of oil and water saturation specifically in the amount of quartz cement, the petrographically determined amounts of quartz cement have been plotted against water saturation, split by grain size (Fig. 22A–C). The very fine- and lower fine-grained sandstones show no systematic variation. The upper fine-grained sands (>177 μm) have the greatest amount of quartz cement (>9%) only in samples with an oil saturation of less than 30% (Fig. 22C); whereas samples with higher saturation tend to have less quartz cement.

5.5. Localised inhibition of quartz cementation

Quartz cement is the most typical cause of porosity-loss in deeply buried sandstones (McBride, 1989). Quartz cementation has been inhibited in the Ula Formation in Tambar as shown by the late onset of quartz cementation (at a high minimum fluid inclusion homogenization temperature) (Fig. 14) and the small amount of quartz cement for the relatively high porosity at a relatively high temperature to which these rocks have been exposed (Figs. 3 and 14).

There are a finite range of factors that have been reported to inhibit quartz cementation. It is possible to exclude the possibility

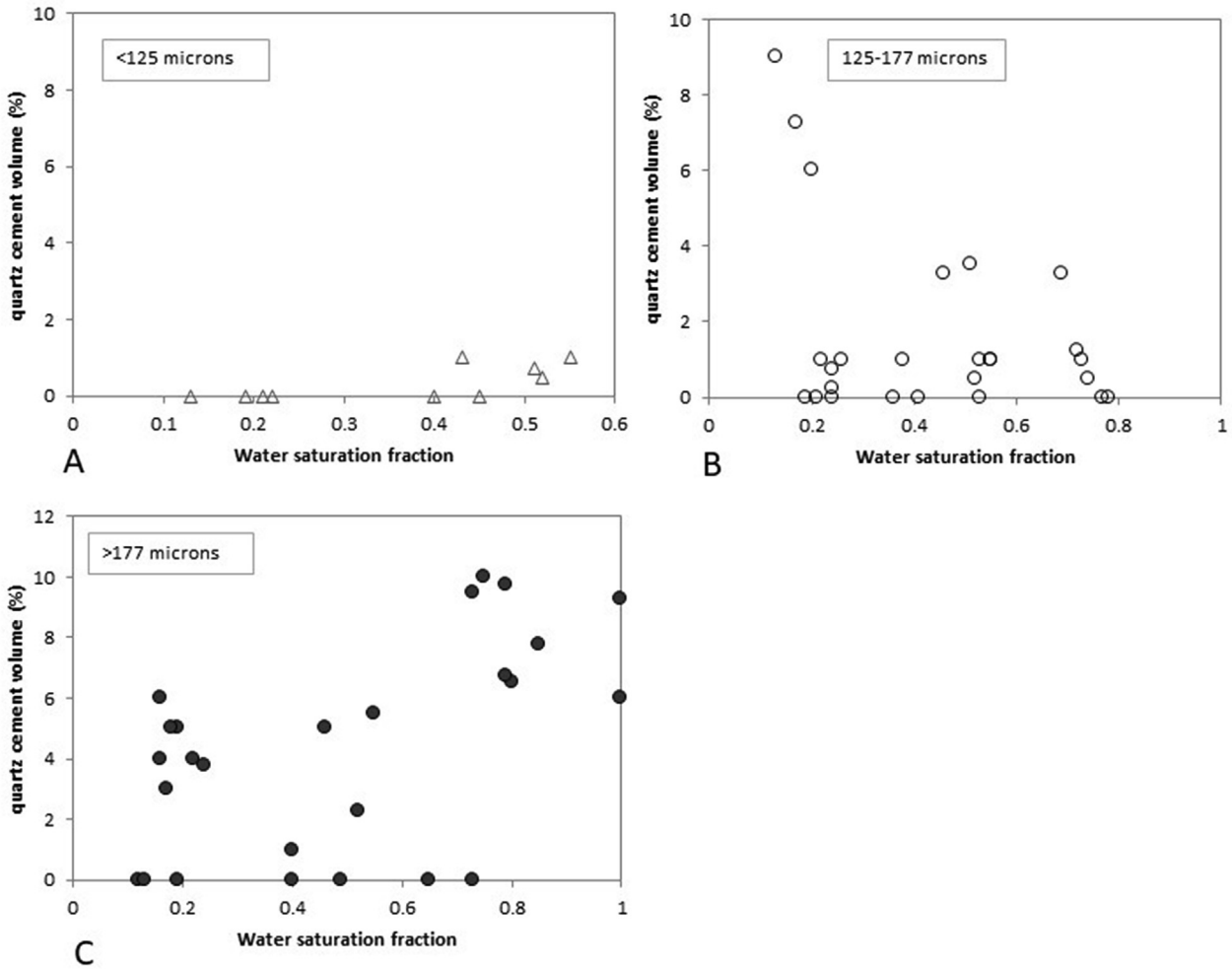

Fig. 22. Water saturation vs. total quartz cement for the three different grain size classes. Only the grain size class of >177 μm show a correlation between high water saturation and high quartz cement volume.

that there is little quartz cement due to the pervasive early fillings of pores with alternative cement; early pore-filling calcite cement is an exception rather than a rule in these sandstones. The remaining options are (Bloch et al., 2002) (i) microcrystalline quartz coatings, (ii) grain-coating chlorite coats, (iii) early emplacement of oil and (iv) overpressure preventing compaction and related pressure solution processes (Sheldon et al., 2003).

Grain-coating microcrystalline quartz has certainly inhibited quartz cementation as revealed by the lack of quartz overgrowth on sand grains that are coated with thick layers of microcrystalline quartz (Fig. 10). Samples with well-developed grain coatings of microcrystalline quartz have the least amounts of quartz cement (Fig. 21C and D). Microcrystalline quartz thus has had an important control on quartz cementation and reservoir quality in these sandstones.

Chlorite is present in these sandstones but it does not occur as well-developed grain coatings. Rather it tends to be highly localised and occurs as pore-filling mats (Fig. 11D). Chlorite grain coatings can be excluded as a primary control on quartz cement abundance.

As for oil to inhibit diagenesis, its emplacement must occur before the diagenetic process under consideration. The relative lack of oil inclusions in quartz suggests that much or most quartz cementation happened before oil charging, i.e., oil charging is in a relatively late process in these sandstones. The addition of oil seems to have had no direct effect on quartz cement abundance in all but the coarsest sandstones (Fig. 22). Indeed, quartz cement is only abundant in the coarsest sandstones with a high water saturation. Oil emplacement seems to have had a role in controlling reservoir quality for some of the Ula Formation sandstones in Tambar.

It is not easy to establish whether overpressure development has had a role in limiting quartz cementation using the empirical data provided, the samples available and the techniques employed. However, these sandstones are reported not to have high fluid pressures (O'Connor et al., 2011) suggesting that overpressure is notan important control on quartz cementation.

5.6. Synthesis of controls on reservoir quality in the Ula Formation in Tambar

The dominant controls on reservoir quality in the Ula Formation in Tambar are the grain size, quartz cementation, total quantity of clay minerals present, oil emplacement and dolomite cement content. These controls combine in different ways in different grain size classes. In general, the lower fine-grained sandstones have the highest porosity and permeability and represent a better reservoir than the very fine-grained sandstones or the upper fine-grained sandstones. Thus coarser grains do not automatically equate to a better reservoir in this case. The mean quartz cement content increases with the increasing grain size (Table 3). The mean feldspar cement content mirrors the quartz cement and presumably is

controlled by similar processes. In contrast, the mean total clay, microcrystalline quartz and dolomite cement contents decrease with the increasing grain size. For the very fine-grained sandstones (<125 μm), the quartz cement and feldspar cement concentrations are very low due to the burial depth and thermal history of these sandstones. Conversely, they have relatively high concentrations of microcrystalline quartz, clay and dolomite. These rocks have a mean porosity relatively high but low permeability due to the pore throat blocking behaviour of clay and dolomite and possibly the microcrystalline quartz given its unusually thick grain coatings (Fig. 10G and H). The presence of oil has had little impact on the very fine-grained sandstones since the later stages of diagenesis (quartz cementation) that occurred after oil charging have little effect on reservoir quality.

For the upper fine-grained sandstones (>177 μm), the quartz cement and feldspar cement concentrations are the highest for the Ula Formation in Tambar but still low given the burial depth and thermal history of these sandstones. They have low concentrations of clay and dolomite and the lowest concentration of microcrystalline quartz (and least well developed grain coats) of all sandstones from Tambar (Table 3). These rocks have a mean porosity and permeability relatively low due to the presence of quartz (and feldspar) cement. These rocks have the greatest amount of quartz cement in samples with the least well-developed microcrystalline quartz grain coatings and a high water saturation (Fig. 21). The presence of oil has had some impact on the upper fine-grained sandstones since the later stages of diagenesis (quartz cementation) that occurred after oil charging have a significant impact on reservoir quality.

The sandstones of the highest porosity and permeability from the Ula Formation at Tambar are the lower fine-grained sandstones (125 μm–177μm) since they have enough microcrystalline quartz to prevent much quartz cementation (and presumably feldspar cementation), but have less dolomite cement and clay compared with the very fine-grained sandstones (Table 3). The presence of oil has had little impact on the lower fine-grained sandstones since the later stages of diagenesis (quartz cementation) that occurred after oil charging had little effect on reservoir quality.

6. Conclusion

The Upper Jurassic Ula Formation in Tambar contains very fine- to fine-grained marine sandstones with an average porosity of 16% despite being buried to a depth of greater than 4000 m and experienced temperatures greater than 160 °C. The main diagenetic cements that had an impact on the reservoir quality of the Ula Formation in Tambar are microcrystalline quartz, quartz overgrowth, illite and dolomite. Microcrystalline quartz is present as thick coatings on sand grains and more abundant than in other marine sandstone reservoirs of the same age in the North Sea Basins. It was sourced from sponge spicules and has a major inhibiting effect on quartz cement growth. Quartz cementation starts at 130 °C, a somewhat higher minimum temperature than many basins, presumably due to the inhibiting effect of microcrystalline quartz. The coarsest-grained sandstones (upper fine) have the least amount of microcrystalline quartz and commensurately the greatest amount of quartz cement. These sandstones have the greatest amount of quartz cement in sandstones with a high water saturation suggesting that the relatively late addition of oil had an impact only on the cleanest and coarsest sandstones. These sandstones have relatively poor reservoir quality due to quartz and feldspar cement growth. The finer sandstones have the greatest quantity of clay and dolomite cement as well as microcrystalline quartz and so are at best, of moderate reservoir quality. It is possible that the extreme quantity of microcrystalline quartz has led to a reduced permeability due to its blocking effect on pore throats.

The intermediate sandstones (lower fine) are of the best reservoir quality due to their abundant microcrystalline quartz coatings, thus inhibiting quartz cement, and less microcrystalline quartz, clay and dolomite compared with the very fine-grained sandstones.

Declaration of competing interest

The authors declare that they have no known competing financial interests or personal relationships that could have appeared to influence the work reported in this paper.

Acknowledgments

This research was funded by Petroleum Technology Development Fund Nigeria.

References

Aase, N.E., Bjorkum, P.A., Nadeau, P.H., 1996. The effect of grain-coating microquartz on preservation of reservoir porosity. AAPG (Am. Assoc. Pet. Geol.) Bull. 80 (10), 1654–1673.
Aase, N.E., Walderhaug, A., 2005. The effect of hydrocarbons on quartz cementation: diagenesis in the Upper Jurassic sandstones of the Miller Field, North Sea, revisited. Petrol. Geosci. 11 (3), 215–223.
Allen, P.A., Mange-Rajetzky, M.A., 1992. Devonian-Carboniferous sedimentary evolution of the Clair area, offshore north-western UK: impact of changing provenance. Mar. Petrol. Geol. 9 (1), 29–52.
Ajdukiewicz, J.M., Nicholson, P.H., Esch, W.L., 2010. Prediction of deep reservoir quality using early diagenetic process models in the Jurassic Norphlet Formation, Gulf of Mexico. AAPG (Am. Assoc. Pet. Geol.) Bull. 94 (8), 1189–1227.
Asquith, G.B., Gibson, C.R., 1982. Basic well log analysis for geologists. Am Assoc Petrol Geologists Methods in Exploration 3, 216.
Barclay, S.A., Worden, R.H., 2000. Geochemical modelling of diagenetic reactions in a sub-arkosic sandstone. Clay Miner. 35 (1), 57–67.
Bergan, M., Tørudbakken, B., Wandås, B., 1989. Lithostratigraphic correlation of Upper Jurassic sandstones within the Norwegian Central Graben: sedimentological and tectonic implications. In: Collinson, J.D. (Ed.), Correlation in Hydrocarbon Exploration. Norwegian Petroleum Society, Graham and Trotman, London, pp. 243–251.
Bjørkum, P.A., Oelkers, E.H., Nadeau, P.H., Walderhaug, O., Murphy, W.M., 1998. Porosity prediction in quartzose sandstones as a function of time, temperature, depth, stylolite frequency, and hydrocarbon saturation. AAPG (Am. Assoc. Pet. Geol.) Bull. 82 (4), 637–648.
Bjorlykke, K., Aagaard, P., Dypvik, H., Hastings, D.S., Harper, A.S., 1988. Diagenesis and reservoir properties of Jurassic sandstones from the Haltenbanken area, offshore mid Norway. In: Spencer, et al. (Eds.), Habitat of Hydrocarbon on the Norwegian ContinentalShelf. Norwegian Petroleum Society Graham and Trotman, pp. 276–286.
Bjørnseth, H.M., Gluyas, J., 1995. Petroleum exploration in the Ula trend: Norwegian. Petrol Soc Special Publ 4, 85–96.
Bloch, S., Lander, R.H., Bonnell, L., 2002. Anomalously high porosity and permeability in deeply buried sandstone reservoirs: origin and predictability. AAPG (Am. Assoc. Pet. Geol.) Bull. 86 (2), 301–328.
Bryant, S., Cade, C., Mellor, D., 1993. Permeability prediction from geologic models. AAPG (Am. Assoc. Pet. Geol.) Bull. 77 (8), 1338–1350.
Burley, S.D., 1984. Patterns of diagenesis in the sherwood sandstoen group (triassic), United Kingdom. Clay Miner. 19 (3), 403–440.
Cade, C.A., Evans, I.J., Bryant, S.L., 1994. Analysis of permeability controls - a new approach. Clay Miner. 29 (4), 491–501.
Chang, J.C., Yortsos, Y.C., 1994. Lamination during silica diagenesis - effects of clay content and Ostwald ripening. Am. J. Sci. 294 (2), 137–172.
Collet, T.S., 1998. Well log characterization of sedimentsporosities in Gas-hydrate bearing reservoirs. In: SPE Annual Technical Conference and Exibition, 27-30 September, New Orleans.
Collet, T.S., Ladd, J., 2000. Detection of Gas-hydrate with downhole logs and assesment of gas-hydrate concentration (saturation) and gas volume on the Black Ridge with electrical resistivity log. In: MATSUMOTO, P.C.K., WALLACE, P.J., DILLON, W.P. (Eds.), Proceedings of the Ocean Drilling Programme Results, vol. 164. U. S. Geological Survey.
Craig, H., 1957. Isotopic standards for carbon and oxygen correction factors for mass spectrometric analysis of carbon dioxide. Geochimeca et Cosmochemica Acta 12.
Dixon, S.A., Summers, D.M., Surdam, R.C., 1989. Diagenesis and preservation of porosity in norphlet formation (upper jurassic), southern Alabama. Am Assoc of Petrol Geol Bull 73 (6), 707–728.
Ehrenberg, S.N., 1990. Relationship between diagenesis and reservoir quality in sandstones of the Garn Formation, Haltenbanken, mid-Norwegian continental shelf. AAPG (Am. Assoc. Pet. Geol.) Bull. 74 (10), 1538–1558.

Evans, J., Cade, C., Bryant, S., 1997. A geological approach to permeability prediction in clastic reservoirs. In: Kupecz, J.A., Gluyas, J., Bloch, S. (Eds.), Reservoir Quality Prediction in Sandstones and Carbonates, vol. 69. AAPG Memoir, pp. 91–102.
Folk, R.L., 1968. Petrology of Sedimentary Rocks. Hemphill, Austin, Texas.
French, M.W., Worden, R.H., Mariani, E., Horn, W.C., Kliewer, C.E., Lamberti, W.A., Mueller, R.R., Fischer, C., 2010. Low temperature porosity preserving microquartz from Upper Cretaceous sandstones of the Subhercynian Basin (Germany). Geochem. Cosmochim. Acta 74 (12). A305-A305.
French, M.W., Worden, R.H., Mariani, E., Larese, R.E., Mueller, R.R., Kliewer, C.E., 2012. Microcrystalline quartz generation and the preservation of porosity in sandstones: evidence from the upper cretaceous of the sub-hercynian basin, Germany. J. Sediment. Res. 82 (5–6), 422–434.
Friedman, I., O'Neil, J.R., 1977. Compilation of Stable Isotope Fractionation Factors of Geochemical Interest, US Geological Survey Professional Papers, Data of Geochemistry.
Gluyas, J.G., Robinson, A.G., Emery, D., Grant, S.M., Oxtoby, N.H., 1993. The link between petroleum emplacement and sandstone cementation. In: Parker, J. (Ed.), Petroleum Geology of the North West Europe, vol. 4. Geological Society of London, pp. 1395–1402.
Haddad, S.C., Worden, R.H., Prior, D.J., Smalley, P.C., 2006. Quartz cement in the Fontainebleau sandstone, Paris basin, France: crystallography and implications for mechanisms of cement growth. J. Sediment. Res. 76 (2), 244–256.
Hamar, G.P., Fjaeran, T., Hesjedal, A., 1983. Jurassic stratigraphy and tectonics of the south-southeastern Norwegian offshore. In: Kaasschieter, J.P.H., Reijers, T.J.A. (Eds.), Petroleum Geology of the Southeastern North Sea and the Adjacent Onshore Areas, vol. 62. Geol. Mijnbouw, pp. 103–114.
Harris, N.B., 2006. Low-porosity haloes at stylolites in the feldspathic Upper Jurassic Ula sandstone, Norwegian North Sea: an integrated petrographic and chemical mass-balance approach. J. Sediment. Res. 76 (3–4), 444–459.
Hogg, A.J.C., Sellier, E., Jourdan, A.J., 1992. Cathodoluminescence of quartz cements in brent group sandstones, alwyn south, UK North Sea. In: Morton, A.C., Hazeldine, S.R. (Eds.), 61. Geological Society, London, Special Publications, pp. 421–440.
Home, P.C., 1987. Ula. In: Spencer, A.M., Holter, E., Campbell, C.J., Hanslein, S.H., Nelsen, P.H.H., Nysteacher, E., Ormaasen, E.G. (Eds.), Geology of the Norwegian Oil and Gas Fields. Graham and Trotman, London, pp. 143–151.
Jahren, J., Ramm, M., 2000. The Porosity preserving effects of microcrystalline quartz coatings in arenitic sandstones: examples from the Norwegian Continental Shelf. In: Worde, R.H., Morad, S. (Eds.), Quartz Cementation in Sandstones, vol. 29. International Association of Sedimentologists Special edition. Blackwell Science, pp. 271–280.
Karlsen, D.A., Nedkvitne, T., Larter, S.R., Bjørlykke, K., 1993. Hydrocarbon composition of authigenic inclusions: application to elucidation of petroleum reservoir filling history. Geochem. Cosmochim. Acta 57 (15), 3641–3659.
Karlsen, D.A., Skeie, J.E., 2006. Petroleum migration, faults and overpressure, part I: calibrating basin modelling using petroleum in traps—a review. J. Petrol. Geol. 29 (3), 227–256.
Knipe, R.J., Anderson, S., Mitchell, A., 1991. Deformation processes and fault seal mechanisms: a combined microstructural analysis from the Ula field, Central Graben, North Sea. AAPG (Am. Assoc. Pet. Geol.) Bull. 75. CONF-910403).
Kraishan, G.M., Rezaee, M.R., Worden, R.H., 2000. Significance of trace element composition of quartz cement as a key to reveal the origin of silica in sandstones: an example from the Cretaceous of the Barrow sub-basin, Western Australia. In: Worden, R.H., Morad, S. (Eds.), Quartz Cementation in Sandstones, vol. 29. International Association of Sedimentologists Special Publications, pp. 317–332.
Land, L.S., 1983. The application of stable isotopes to studies of the origin of dolomite and to problems of diagenesis of clastic sediments, Society of Economic Paleontologists and Mineralogists, Short course, Stable isotopes in sedimentary geology. In: Stable Isotopes in Sedimentary Geology, vol. 4, pp. 1–4.22.
Lima, R.D., De Ros, L.F., 2002. The role of depositional setting and diagenesis on the reservoir quality of Devonian sandstones from the Solimões Basin, Brazilian Amazonia. Mar. Petrol. Geol. 19 (9), 1047–1071.
Macaulay, C.I., Fallick, A., McLaughlin, O.M., Haszeldine, R.S., Pearson, M.J., 1998. The significance of d13C of carbonate cement in reservoir sandstones; a regional perspective from the Jurassic of the Northern North Sea. In: Morad, S. (Ed.), Carbonate Cementation in Sandstones, vol. 26. International Association of Sedimentologists Special Publications, pp. 395–408.
Marchand, A.M.E., Haszeldine, R.S., Smalley, P.C., Macaulay, C.I., Fallick, A.E., 2001. Evidence for reduced quartz-cementation rates in oil-filled sandstones. Geology 29 (10), 915–918.
McBride, E.F., 1989. Quartz cement in sandstones: a review. Earth Sci. Rev. 26 (C), 69–112.
Molenaar, N., Cyziene, J., Sliaupa, S., 2007. Quartz cementation mechanisms and porosity variation in Baltic Cambrian sandstones. Sediment. Geol. 195 (3), 135–159.
Morad, S., Al-Ramadan, K., Ketzer, J.M., De Ros, L.F., 2010. The impact of diagenesis on the heterogeneity of sandstone reservoirs: a review of the role of depositional facies and sequence stratigraphy. AAPG (Am. Assoc. Pet. Geol.) Bull. 94 (8), 1267–1309.
Morad, S., Ketzer, J.M., De Ross, L.F., 2012. Linking diagenesis to sequence stratigraphy: an integrated tool for understanding and predicting reservoir quality distribution. In: Morad, S., KETZER, J.M., DE, R.O.S.S. (Eds.), Linking Diagenesis to Sequence Stratigraphy. Special Publication of the International Association of Sedimentologists, vol. 45. John Wiley and Sons, Chichester, pp. 1–36.
Nedkvitne, T., Karlsen, D.A., Bjorlykke, K., Larter, S.R., 1993. Relationship between reservoir diagenetic evolution and petroleum emplacement in the Ula Field, North Sea. Mar. Petrol. Geol. 10 (3), 255–270.
O'Connor, S., Rasmussen, H., Swarbrick, R., Wood, J., 2011. Integrating a hydrodynamically-titled OWC and a salt-withdrawal depositional model to explore the Ula Trend. Geofluids 11 (4), 388–400.
O'Neil, J.R., Epstein, S., 1966. Oxygen isotope fractionation in the system dolomite-calcite-carbon dioxide. Science 152 (3719), 198–201.
Oelkers, E.H., Bjorkum, P.A., Murphy, W.M., 1996. A petrographic and computational investigation of quartz cementation and porosity reduction in North Sea sandstones. Am. J. Sci. 296 (4), 420–452.
Osborne, M.J., Swarbrick, R.E., 1999. Diagenesis in North Sea HPHT elastic reservoirs - consequences for porosity and overpressure prediction. Mar. Petrol. Geol. 16 (4), 337–353.
Oxtoby, N.H., 1994. The Ula field. In: Warren, E.A., Smalley, P.C. (Eds.), North Sea Formation Waters: London, vol. 15. The Geological Society London, Memoir, p. 74.
Oxtoby, N.H., Mitchell, A.W., Gluyas, J.G., 1995. The filling and emptying of the Ula Oilfield: fluid inclusion constraints. In: Cubitt, J.M., England, W.A. (Eds.), The Geochemistry of Reservoirs, vol. 86. Geological Society, London, Special Publications, pp. 141–157.
Partington, M.A., Mitchener, B.C., Milton, N.J., Fraser, A.J., 1993. Genetic sequence stratigraphy for the north sea late jurassic and early cretaceous: distribution and prediction of kimmeridgian–late ryazanian reservoirs in the north sea and adjacent areas. Geol Soc London 4, 347–370.
Petersen, H.I., Andersen, C., Holme, A.C., Carr, A.D., Thomsen, E., 1 October 2012. Vitrinite reflectance gradients of deep wells with thick chalk sections and high pressure: implications for source rock maturation, Danish-Norwegian Central Graben, North Sea. Man Int. J. Coal Geol. 100, 65–81.
Ramm, M., 1992. Porosity depth trends in reservoir sandstones - theoretical models related to Jurassic sandstones offshore Norway. Mar. Petrol. Geol. 9 (5), 553–567.
Ramm, M., Bjorlykke, K., 1994. Porosity depth trends in Norwegain reservoirs - assessing the quantitativ effects of varying pore-pressure, temperature history and mineralogy, Norwegian shelf data. Clay Miner. 29 (4), 475–490.
Ramm, M., Forsberg, A.W., Jahren, J., 1997. Porosity-depth trends in deeply buried Upper Jurassic Reservoirs in the Norwegian Central Graben: an example of porosity preservation beneath the normal economic basement by grain coating microquartz. In: Kupecz, J.A., Gluyas, J., Bloch, S. (Eds.), Reservoir Quality Prediction in Sandstones and Carbonates, vol. 69. AAPG Memoir, pp. 177–200.
Rider, M., Kennedy, M., 2011. The Geological Interpretation of Well Logs, 3rd Edition. Rider French consulting Limited, Glasgow, p. 432.
Rosenbaum, J., Sheppard, S.M.F., 1986. An isotopic study of siderites, dolomites and ankerites at high temperatures. Geochem. Cosmochim. Acta 50 (6), 1147–1150.
Schmid, S., Worden, R.H., Fisher, Q.J., 2004. Diagenesis and reservoir quality of the sherwood sandstone (triassic), corrib field, slyne basin, west of Ireland. Mar. Petrol. Geol. 21 (3), 299–315.
Serra, O., 1984. Fundamentals of well log interpretation. In: The Acquisition of Logging Data. Dev. Pet. Sci; 15A, vol. 1. Elsevier, Amsterdam.
Sheldon, H.A., Wheeler, J., Worden, R.H., Cheadle, M.J., 2003. An analysis of the roles of stress, temperature, and pH in chemical compaction of sandstones. J. Sediment. Res. 73 (1), 64–71.
Skjerven, J., Rijs, F., Kalheim, J., 1983. Late paleozoic to early cenozoic structural development of the south-southeastern Norwegian North Sea. Geol. Mijnbouw 62, 35–45.
Stewart, I.J., 1993. Structural controls on the late jurassic age shelf system, Ula trend, Norwegian North Sea. Geol Soc London 4, 469–483.
Stokkendal, J., Friis, H., Svendsen, J.B., Poulsen, M.L.K., Hamberg, L., 2009. Predictive permeability variations in a hermod sand reservoir, stine segments, siri field, Danish North Sea. Mar. Petrol. Geol. 26 (3), 397–415.
Underhill, J.R., 1998. Jurassic. In: Glennie, K.W. (Ed.), Petroleum Geology of the North Sea:Basic Concepts and Recent Advances. Blackwell Science, p. 656.
Vagle, G.B., Hurst, A., Dypvik, H., 1994. Origin of quartz cements in some sandstones from the jurassic of the inner moray firth (UK). Sedimentology 41 (2), 363–377.
Veizer, J., Ala, D., Azmy, K., Bruckschen, P., Buhl, D., Bruhn, F., Carden, G.A.F., Diener, A., Ebneth, S., Godderis, Y., Jasper, T., Korte, C., Pawellek, F., Podlaha, O.G., Strauss, H., 1999. Sr-87/Sr-86, delta C-13 and delta O-18 evolution of Phanerozoic seawater. Chem. Geol. 161 (1–3), 59–88.
Walderhaug, O., 1994. Temperatures of quartz cementation in Jurassic sandstones from the Norwegian continental shelf - evidence from fluid inclusions. J. Sediment. Res. B Stratigr. Global Stud. 64 (2), 311–323.
Walderhaug, O., Lander, R.H., Bjorkum, P.A., Oelkers, E.H., Bjorlykke, K., Nadeau, P.H., 2000. Modelling quartz cementation and porosity in reservoir sandstones: examples from the Norwegain continental shelf. In: Worden, R.H., Morad, S. (Eds.), Quartz Cementation in Sandstones, vol. 29. International Association of Sedimentologists Special Publications, pp. 39–50.
Warren, E.A., Smalley, C.P., Howarth, R.J., 1994. Compositional variations of North Sea formation waters. Mem. Geol. Soc. Lond. 15, 119–208.
Weibel, R., Friis, H., Kazerouni, A.M., Svendsen, J.B., Stokkendal, J., Poulsen, M.L.K., 2010. Development of early diagenetic silica and quartz morphologies - examples from the siri canyon, Danish North Sea. Sediment. Geol. 228 (3–4), 151–170.
Wilhelms, A., Larter, S.R., 1994. Origin of tar mats in petroleum reservoirs. Part II: formation mechanisms for tar mats. Mar. Petrol. Geol. 11 (4), 442–456.
Wilkinson, M., Haszeldine, R.S., 2011. Oil charge preserves exceptional porosity in

deeply buried, overpressured, sandstones: Central North Sea, UK. J. Geol. Soc. 168 (6), 1285–1295.
Williams, L.A., Crerar, D.A., 1985. Silica diagenesis; II, General mechanisms. J. Sediment. Res. 55 (3), 312–321.
Williams, L.A., Parks, G.A., Crerar, D.A., 1985. Silica diagenesis; I, Solubility controls. J. Sediment. Res. 55 (3), 301–311.
Worden, R.H., Burley, S.D., 2003. Sandstone diagenesis: the evolution from sand to stone. In: Burley, S.D., Worden, R.H. (Eds.), Sandstone Diagenesis, Recent and Ancient, vol. 4. International Association of Sedimentologists Reprint Series, pp. 3–44.
Worden, R.H., French, M.W., Mariani, E., 2012. Amorphous silica nanofilms result in growth of misoriented microcrystalline quartz cement maintaining porosity in deeply buried sandstones. Geology 40 (2), 179–182.
Worden, R.H., Morad, S., 2003. Clay minerals in sandstones: controls on formation, distribution and evolution. In: Worden, R.H., Morad, S. (Eds.), Clay Mineral Cements in Sandstones, vol. 34. International Association of Sedimentologists Special Publications, pp. 3–41.
Worden, R.H., Bukar, M., Shell, P., 2018. The effect of oil emplacement in deeply buried sandstone reservoir. Am. Assoc. Petrol. Geol. Bull. 102 (1), 49–75.
Worden, R.H., Oxtoby, N.H., Smalley, P.C., 1998. Can oil emplacement prevent quartz cementation in sandstones? Petrol. Geosci. 4 (2), 129–137.
Worden, R.H., Warren, E.A., Smalley, P.C., Primmer, T.J., Oxtoby, N.H., 1995. Evidence for resetting of fluid inclusions from quartz cements in oil fields - Discussion. Mar. Petrol. Geol. 12 (5), 566–570.
Worden, R.H., Armitage, P.J., Butcher, J.M., Churchill, J.M., Csoma, A.E., Hollis, C., Lander, R.H., Omma, J.E., 2020. Petroleum reservoir quality prediction. overview and contrasting approaches from sandstone and carbonate communities. Geol Soc of London Special Publ 435, 1–31.